Rostrocaudal Patterning and Neural Crest Differentiation of Human Pre-Neural Spinal Cord Progenitors *in vitro*

Fay Cooper[1,*], George E Gentsch[1], Richard Mitter[2], Camille Bouissou[1], Lyn Healy[3], Ana Hernandez-Rodriguez[1], James C Smith[1] and Andreia S Bernardo[1,4]

[1]Developmental Biology Laboratory, The Francis Crick Institute, 1 Midland Road, London, NW1 1AT, UK
[2]Bioinformatics & Biostatistics Core Facility, The Francis Crick Institute, 1 Midland Road, London, NW1 1AT, UK
[3]Human Embryo and Stem Cell Unit, The Francis Crick Institute, 1 Midland Road, London, NW1 1AT, UK
[4]National Heart and Lung Institute, Imperial College London, UK

*Corresponding author

ABSTRACT

The spinal cord emerges from a niche of neuromesodermal progenitors (NMPs) formed and maintained by Wnt/FGF signals in the posterior end of the embryo. NMPs can be generated from human pluripotent stem cells and hold promise for spinal cord replacement therapies. However, NMPs are transient and unable to produce the full range of rostrocaudal spinal cord identities *in vitro*. Here we report the generation of NMP-derived pre-neural progenitors (PNPs) with stem cell-like self-renewal capacity. PNPs maintain pre-spinal cord identity by co-expressing the transcription factors SOX2 and CDX2, and they lose the mesodermal potential by downregulating TBXT. Over 10 passages these cells divide to self-renew and to make trunk neural crest, while gradually adopting a more posterior identity by activating colinear *HOX* gene expression. Rostrocaudal identity can be prolonged in a thoracic identity for up to 15 passages by modulating TGF-β, and PNPs can be ventralised by Hedgehog signalling.

INTRODUCTION

Neural stem cells (NSCs) are a useful *in vitro* tool for understanding neural development and disease, and they have great potential for use in regenerative medicine (Snyder, 2017). However, for use in cell replacement therapy, it is important that NSCs adopt the correct region-specific identities and adapt properly to their local microenvironments (Kadoya et al., 2016; Kumamaru et al., 2018; Nagoshi, Tsuji, Nakamura, & Okano, 2019). This requirement for specific neural subtypes is illustrated by patients with motor neuron disease or spinal cord injuries, who often have lesions in specific neuronal cell types and whose treatment depends on developing protocols that cause induced pluripotent stem

cells (iPSCs) to differentiate into the right neural subtypes (Nijssen, Comley, & Hedlund, 2017; Trawczynski, Liu, David, & Fessler, 2019).

The development of these protocols will be informed by our understanding of neurogenesis. Forebrain and midbrain develop from the anterior neural plate, a naïve tissue neuralised by the underlying axial mesoderm through the release of TGF-β inhibitors (Cajal et al., 2012; Mathis & Nicolas, 2000). Spinal cord arises from a progenitor pool of neuromesodermal progenitors (NMPs) that reside in the caudal lateral epiblast/node streak border and later the chordoneural hinge (Wilson, Olivera-Martinez, & Storey, 2009). NMPs are bi-potent and give rise to both the posterior neural tube and adjacent somite-forming paraxial mesoderm (Brown & Storey, 2000; Cambray & Wilson, 2002, 2007; Delfino-Machin, Lunn, Breitkreuz, Akai, & Storey, 2005; Tzouanacou, Wegener, Wymeersch, Wilson, & Nicolas, 2009). NMPs are maintained by the synergistic action of FGF and Wnt signals which activate the co-expression of the transcription factors TBXT, SOX2 and CDX2. TBXT and SOX2 are mutually antagonistic cell fate determinants for the mesodermal and neuroectodermal germ layers, respectively (Gouti et al., 2017; Henrique, Abranches, Verrier, & Storey, 2015; Koch et al., 2017; Tsakiridis et al., 2014; Wymeersch et al., 2016). CDX2 conveys increasingly more posterior identity to NMP descendants by inducing colinear *HOX(1-13)* gene expression during axial elongation (Amin et al., 2016; Neijts, Amin, van Rooijen, & Deschamps, 2017; van de Ven et al., 2011; van den Akker et al., 2002). The human HOX genes are expressed in a spatial and temporal order that is colinear with their physical 3' to 5' genomic position, and assign overlapping regional identity to the brain and vertebral segments of the spinal cord: HOX1-5, hindbrain; HOX4-6, cervical; HOX6-9, thoracic and HOX10-13, lumbosacral (Philippidou & Dasen, 2013).

As the rostrocaudal axis elongates, NMPs that enter the primitive streak downregulate SOX2, upregulate TBX6, and contribute to the developing somites (Javali et al., 2017; Takemoto et al., 2011). In contrast, neural commitment begins in the pre-neural tube (PNT), located immediately rostral to the NMP niche (Ruth Diez del Corral, Breitkreuz, & Storey, 2002). In the PNT, cells no longer express *TBXT*, but maintain expression of *SOX2* and *NKX1-2* (I. Olivera-Martinez & Storey, 2007; Storey et al., 1998). Neurogenic genes such as *PAX6* and *NEUROG2* are not upregulated in this region due to repression from the continued FGF signalling (R. Diez del Corral et al., 2003; Lunn, Fishwick, Halley, & Storey, 2007). The next step of neural commitment is prompted by the exposure of cells to retinoic acid (RA) from the adjacent somites as they migrate out of the PNT region and into the neural tube. The switch from FGF to RA signalling alleviates repression of the neural transcription factors *PAX6* and

IRX3 and down regulates *NKX1-2* (R. Diez del Corral et al., 2003; Sasai, Kutejova, & Briscoe, 2014; Shum et al., 1999).

Attempts have been made *in vitro* to recapitulate the developmental pathways leading to anterior or posterior NSCs. Anterior NSCs can be generated from hPSCs via dual TGF-β (Activin/BMP) inhibition (Chambers et al., 2009). Initial attempts to generate spinal cord progenitors relied on posteriorising anterior NSCs through exposure to retinoic acid or Wnt and FGF treatments (Lee et al., 2007; X. J. Li et al., 2005; Mazzoni et al., 2013; Peljto, Dasen, Mazzoni, Jessell, & Wichterle, 2010; Wichterle, Lieberam, Porter, & Jessell, 2002). However, this yielded neural derivatives as far posterior as hindbrain and upper cervical regions, primarily through saltatory expression of *HOX(1-5)* genes, but did not yield spinal cord progenitors with thoracic or lumbar identities. Consistent with *in vivo* evidence, combined Wnt and FGF stimulation efficiently converted mouse or human PSCs into NMP-like cells, which are becoming a promising source to make spinal cord tissue for cell replacement therapies (Frith et al., 2018; Gouti et al., 2014; Lippmann et al., 2015; Turner et al., 2014; Verrier, Davidson, Gierlinski, Dady, & Storey, 2018). However, *in vitro* derived NMPs are difficult to maintain and often fail to trigger the full range of HOX-mediated regionalisation along the rostrocaudal axis. Thus, few protocols have been developed that generate all rostrocaudal regions (cervical, thoracic, lumbar and sacral) of the spinal cord (Kumamaru et al., 2018; Lippmann et al., 2015). Here we describe *in vitro* conditions which commit NMPs to pre-neural progenitors (PNPs). These PNPs are stable for up to 10 passages (30 days) and can also generate neural crest (NC) derivatives across a full range of rostrocaudal identities. PNPs can be locked in a thoracic identity and maintained long term in culture by the addition of TGFβ inhibitors to the medium. Furthermore, PNPs can give rise to a variety of spinal cord derivatives, including motor neuron and interneuron subtypes, through the addition of a sonic hedgehog (SHH) agonist. Our protocol will advance research into spinal cord replacement therapy and in-depth modelling of both spinal cord and neural crest disorders.

RESULTS

Optimising the generation of NMP-like cells from hPSCs through Wnt modulation

Previous studies have shown that Wnt/FGF signalling causes mouse and human PSCs to adopt neuromesodermal bipotency (Frith et al., 2018; Gouti et al., 2014; Lippmann et al., 2015; Turner et al., 2014; Verrier et al., 2018). Human NMP protocols differ in both the magnitude and time window of Wnt stimulation, as well as with respect to the addition of other signal modulators including FGF (Figure 1 - figure supplement 1A)(Denham et al., 2015; Edri, Hayward, Baillie-Johnson, Steventon, & Martinez Arias, 2019; Frith et al., 2018; Gomez et al., 2019; Gouti et al., 2014; Kumamaru et al., 2018;

Lippmann et al., 2015; Verrier et al., 2018; Wang et al., 2019). To find the critical Wnt signalling threshold for the generation of NMP-like cells from the WA09 (H9) hESC line, cells were seeded at a fixed density and 24h later exposed to increasing concentrations of the canonical Wnt agonist CHIR99021 (CHIR) while keeping FGF2 ligands constant (Figure 1A). Our culture medium lacked the retinoic acid (RA) precursor vitamin A (retinol) and contained the pan-RA receptor (RAR) inverse agonist AGN193109 (AGN) (Klein et al., 1996). RA neuralises multipotent cells, so its degradation by CYP26A1 is essential for NMP maintenance (Abu-Abed et al., 2001; Benjamin L. Martin & Kimelman, 2010; Sakai et al., 2001). Yet, the RA receptor gamma (RARγ) is highly expressed in NMPs suggesting that transcriptional repression mediated by RARγ in the absence of its ligand supports NMPs and axial elongation (Amanda Janesick et al., 2014). AGN addition reduced aldehyde dehydrogenase (ALDH) activity suggesting that endogenous RA synthesis was inhibited (Figure 1 – figure supplement 1B).

After 36h, when cultures reached confluency, cells were analysed for SOX2, TBXT and CDX2 expression by immunofluorescence (Figure 1B,C). Low concentrations of CHIR (0-1µM) caused cells to express high SOX2 and to be negative for TBXT and CDX2. At 3µM CHIR, TBXT and CDX2 protein became detectable in some cells. At 5-10µM CHIR, TBXT and CDX2 levels were further elevated, while SOX2 expression decreased with increasing concentrations of CHIR. Bearing in mind the role of POU5F1 (also known as OCT4) in maintaining pluripotency and axis elongation (Aires et al., 2016; Gouti et al., 2017), we also analysed expression of this protein at increasing CHIR concentrations. As expected, when cells were treated with rising CHIR concentrations, OCT4 expression was lost (Figure 1-figure supplement 1C,D). Based on the co-expression of OCT4, SOX2, CDX2 and TBXT proteins, we determined that 5µM CHIR was the optimal concentration to generate NMPs using H9 hESCs at this cell density. We could also reliably generate NMP-like cells from WA01 (H1) hESCs and the AICS-ZO1-GFP iPSC line, which also required intermediate (but different) levels of Wnt activation (Figure 1 – figure supplement 2A,B). These data show that optimising the magnitude of Wnt signalling is important for obtaining NMP-like cells from different PSC lines.

Transcriptional profiling reveals a common NMP gene set

To further characterise our NMP-like cells, Wnt/FGF-induced transcriptional changes in H9 hPSCs were quantified by bulk RNA sequencing (RNA-Seq) after 36h. 1,367 genes were significantly differentially expressed between hESC and NMP stages (445 up and 922 down; FDR <1%, a fold change of at least ± 2, and a base mean >100) (Supplementary file 1). The biological processes most significantly enriched within upregulated genes included ‘anterior-posterior pattern specification’ and ‘regionalisation’, processes which reflect the roles of NMPs *in vivo* (Figure 1D). To define a common gene set expressed

by *in vitro* NMPs, we compared our gene list of upregulated genes with two other NMP-related gene expression studies (Frith et al., 2018; Verrier et al., 2018). The comparison revealed 26 genes that were consistently upregulated in all three studies (Figure 1E, F). Among these were well-established NMP markers such as TBXT, WNT8A, CDX2, FGF17, FST and NKX1-2 (Figure 1F). Several novel genes were also identified, including AC007277.3, a long non-coding transcript, and TTC29 and EGFLAM, all of which may be useful as NMP markers. Overall, our results show that hPSC-derived NMPs generated in the absence of RA signalling express known *in vivo* NMP marker genes and share a distinct gene signature with other *in vitro* hPSC-derived NMPs.

Prolonged culture of NMPs results in loss of mesodermal potency and the emergence of epithelial SOX2$^+$/CDX2$^+$ colonies

NMPs have previously been maintained in culture for up to seven days (Lippmann et al., 2015), but it is necessary to culture them for longer than this to create enough cells for developmental and therapeutic assays. We sought to extend the culture of spinal cord progenitors by generating the posterior (SOX2$^+$/CDX2$^+$) equivalent of anterior (SOX2$^+$/OTX2$^+$) NSCs. To this end we dissociated and replated NMP-like cells at low density at 36h, supressed RA signalling (by removal of vitamin A from the medium and treatment with AGN) and continued Wnt/FGF treatment to minimise mesodermal commitment while halting early neural commitment (Figure 2A).

Using immunofluorescence and RT-qPCR, we showed that these culture conditions maintain a SOX2$^+$/CDX2$^+$ cell population for up to 10 passages, corresponding to ~30 days (Figure 2B,C). After one passage (P1) the cultures were heterogeneous with some cells expressing the NMP-characteristic TBXT$^+$/SOX2$^+$/CDX2$^+$ signature. By P3, TBXT and its immediate downstream target TBX6 were undetectable, but most cells continued to express CDX2 and SOX2, suggesting a loss of mesodermal and a maintenance of neural potency (Figure 2B-D). Over time, the number of SOX2$^+$/CDX2$^+$ cells decreased and *SOX2/CDX2* transcript levels were dramatically reduced (Figure 2B,C). Replicate experiments showed the same trend, but the downregulation of *CDX2/SOX2* transcripts occurred at different rates (Figure 2 - figure supplement 1A,B).

By P5, the cell population had segregated into two types, as judged by bright-field and immunofluorescence imaging (Figure 2B and 2E): one formed compact SOX2$^+$/CDX2$^+$ cell colonies, while the other was negative for SOX2/CDX2 and had acquired mesenchymal characteristics such as cell spreading and SNAI1 expression (Figure 2F). The SOX2$^+$/CDX2$^+$ cells appeared to be epithelial, based on the accumulation of mEGFP-tagged zona occludens (ZO)-1 at tight junctions in transgenic

AICS iPSCs (Figure 2G). Together, our results showed that prolonged exposure of hPSCs to Wnt/FGF signalling with inhibition of RA signalling generates a semi-stable epithelial $SOX2^+/CDX2^+$ progenitor population that could be maintained for up to 10 passages.

NMPs form neural progenitors and neural crest derivatives over time

To investigate gene expression changes during the transition of NMP-like cells into epithelial and mesenchymal populations, we profiled the transcriptomes of our cultures by bulk RNA-Seq across twelve time points from 24h after seeding hESCs (time 0, t0) to P10. Analysis of principle components 1 and 2 (PC1 and PC2) showed that most biological replicates (n=2-3) clustered together and PC1 (43% variation) separated according to the duration between time points (Figure 3–figure supplement 1A). Some outliers were identified, which we presume to be a reflection of biological variation in our experiments. In support of this, outliers such P1.r1 and P2.r1 associated with the previous passage, such that P2.r1 clustered more closely to P1.r2 and P1.r3, suggesting that replicate 1 (r1) differentiated through the same transitions, but at a slower pace than r2 and r3.

Next, k-means hierarchical clustering was applied to all gene-specific profiles that were significantly different over at least two consecutive time points. Each of the gene clusters showed a distinct transcriptional behaviour over time (Figure 3A, Supplementary file 2). The genes of each cluster were analysed for enriched gene associated biological processes and the most significant four biological process gene ontology terms are listed in Figure 3B (Supplementary file 3). Clusters 2 (C2) and 6 (C6) showed elevated gene expression from P1 to P8, when cells robustly expressed SOX2 and CDX2. Consistent with the role of CDX2 in regulating colinear *HOX* gene expression, *CDX2* and *HOX(1-9)* genes were grouped together in C2, which showed 'regionalization' as the most enriched biological process (Amin et al., 2016; Neijts et al., 2017). Conversely, *SOX2* was clustered with other neural fate determinants including *SOX21, SP8* and *GBX2* in C6 (X. Li, Liu, Qiu, & Yang, 2014; Luu, Ellisor, & Zervas, 2011; Sandberg, Kallstrom, & Muhr, 2005). Not surprisingly, this cluster was linked strongly with various biological functions of neurogenesis. As expected, the most posterior HOX genes were found in C4 and C9, which showed a peak of expression around P7-P8 and P9-P10, respectively. This was in line with previous findings indicating *HOX13* genes retro-inhibit anterior *HOX* and *CDX2* transcription (Denans, Iimura, & Pourquie, 2015). Thus, we observed full colinear *HOX(1-13)* gene expression across ten passages (Figures 3C,D). The onset of terminal *HOX* gene expression varied in later passages, possibly reflecting slight variation in differentiation rates between experiments (Figure 3A,C, Figure 3– figure supplement 2A,B). In parallel with the onset of terminal HOX expression, C4 and C9 included genes with elevated expression at P9 and P10 (Figure 3A). These clusters were enriched for differentiated tissues such as the skeletal system (C9) and the circulatory system (C4) suggesting that

cells at P7/P8 start to differentiate and this provides a genetic explanation for the decrease in cell viability and the increase in cell spreading at late passages (Figure 3A,B,E).

Similar to C4, C1 consisted of genes upregulated at P9/P10. C1 and C4 genes were enriched for cell death, cell migration and neural crest-related biological processes such as ossification, suggesting some loss of cell viability and the onset of cell differentiation in these later passages (Figure 3A,B). Together, these results suggest that cells become neural crest-like and then terminally differentiate, which would be in keeping with the crest-related tissue types identified within the GO term analysis of C4 and C9. This is also consistent with the decrease in cell viability, which we observe towards passage 10. Thus, NMPs form neural progenitors that become more posterior over time, together with subpopulations of migratory neural crest (NC) cells.

NMP-derived cells stabilise as epithelial pre-neural progenitors

To determine the extent to which NMP-derived cells undergo differentiation, epithelial and mesenchymal cells were enzymatically separated at P5, profiled by bulk RNA-Seq, and compared with the original NMP-like transcriptional profiles (Figure 4 - figure supplement 1A). The temporal progression from 36h to P5 accounted for the majority of gene variation (PC1, ~70%) that was detected. The lineage bifurcation of NMP descendants led to the identification of 907 differentially expressed genes between epithelial and mesenchymal cells (426 genes up in epithelial and 481 genes up in mesenchymal cells; FDR <1%, ≥2-fold change, DESeq2 base mean >100 reads—supplementary file 4). Strikingly, the enrichment analysis of upregulated genes for cellular component GO terms showed that epithelial and mesenchymal cells were linked to key attributes of nerve cell differentiation (e.g. ‘synapse’ and ‘axon’) and neural crest cell migration (e.g. ‘extracellular matrix’ and ‘adherens junction’), respectively (Figure 4A,B). Molecular function GO terms for both samples were similar, and primarily reflected the large number of transcription factors expressed, but also included ‘growth factor binding’ terms which represented WNT/FGF signalling genes in addition to TGFβ superfamily signalling genes (Supplementary file 5). Few of these genes were differentially expressed between epithelial and mesenchymal samples, and they included both positive (BMP4/5/7) and negative (GREM1 and CER1) regulators of TGFβ signalling (Figure 4 – figure supplement 1B, Supplementary file 5). Together this analysis further suggests that the epithelial cells, unlike the mesenchymal cells, are a neuronal cell type and that endogenous signalling events influence cell identity over time.

Next, a panel of previously established NMP, pre-neural progenitors (PNP) and neural progenitor (NP) marker genes were used to pinpoint neural progression *in vitro* (Isabel Olivera-Martinez et al., 2014; Ribes et al., 2008; Verrier et al., 2018). As expected, 36h cells were positive for NMP markers (*FGF8*, *WNT3A* and *TBXT*) and NMP/PNP (*SOX2*, *NKX1-2* and *WNT8A/C*), while the NP determinants *PAX6, IRX3* and *SOX1* were hardly transcribed (Figure 4C). By P5, epithelial cells had lost most NMP-exclusive expression, while the PNP markers *SOX2* and *NKX1-2* were retained (Figure 4D). *NEUROG2* and FGFR2, two PNT/NT markers, were also active in P5 epithelial cells (Isabel Olivera-Martinez et al., 2014; Ribes et al., 2008). Furthermore, neural progenitor markers were low or absent in epithelial P5 cells (Figure 4D). Immunofluorescence for TBXT, SOX2 and PAX6 confirmed this transcriptional analysis, some of which was further validated by RT-qPCR (Figure 4 – figure supplement 1C). Together, we find that epithelial colonies have a PNP identity and do not express key neural maturation genes.

NMP-derived mesenchymal cells are NC

We next sought to determine the identity of the mesenchymal cells. *In vitro* studies have revealed that NMPs can become trunk NC cells, a migratory mesenchymal cell population which goes on to form tissues including cartilage, bone and smooth muscle (Frith et al., 2018; Hackland et al., 2019; Leung et al., 2016). Moreover, our bulk RNA-Seq suggested that over passaging there was an increase in genes associated with cell migration and NC derivatives, concomitant with the reduction of epithelial cells and increase of differentiating mesenchymal cells in late passages (Figures 2E and 3A,B). Thus, we first determined whether mesenchymal P5 cells had acquired NC-specific gene expression. Transcriptome-wide analysis showed that several NC markers genes, including *SNAI1, SOX9* and *SOX10,* were significantly higher in mesenchymal cells compared with their epithelial PNP counterparts (Figure 5A). This was corroborated by immunofluorescence of P5 tissue cultures, which showed SNAI1$^+$ and SOX10$^+$ mesenchymal cells scattered between SOX2$^+$/CDX2$^+$ PNP colonies (Figures 2B and 5B). In support of a posterior NC identity, mesenchymal P5 and P8 cells progressively expressed more posterior *HOX* genes, mirroring the PNP rostrocaudal identity (Figure 3C). By contrast, the cranial NC marker ETS1 was only detectable in a few mesenchymal cells (Figure 5C). To determine if mesenchymal cells were capable of generating NC derivatives, mesenchymal P5 cells were exposed to 1% fetal calf serum (FCS) for 7 days to convert them into NC-derived vasculature smooth muscle, containing cytoplasmic fibres of α-smooth muscle actin (α-SMA also known as ACTA2; Figure 5D,E) (Mohlin et al., 2019). Together, these results show that the mesenchymal cells surrounding PNPs are functional posterior NC cells.

NMP-derived trunk PNPs are stem cell-like and give rise to migratory NC

The immunofluorescence analysis of fixed PNP/NC cell cultures revealed that some nuclei found within tightly clustered PNP colonies were negative for CDX2, but positive for SNAI1, suggesting that they are undergoing epithelial-to-mesenchymal transition (EMT) and becoming NC cells (Cano et al., 2000; Simoes-Costa & Bronner, 2015) (Figure 6A, 2B,E). To test this idea, PNP colonies ($CDX2^+/SNAI1^-$) purified from NC cells using selective detachment were sub-cultured for four passages (P+1 to P+4) (Figure 6B). Immunofluorescence staining showed that, despite the near complete absence of $SNAI1^+$ NC cells in P+1 cultures, by P+4 30% of the cells were mesenchymal ($CDX2^-/SNAI1^+$) suggesting that PNPs undergo EMT to generate NC cells (Figure 6B,C). To exclude the possibility that after PNP purification, a few remaining NC cells repopulate the culture over passaging, single PNP or NC cells were plated by fluorescence-activated cell sorting (FACS) into single wells (Figure 6 - figure supplement 1A). No colonies arose from single NC cells, suggesting that these cells have limited proliferative capacity. By contrast, single PNPs gave rise to clonal cell lines which consisted of epithelial colonies ($CDX2^+/SOX2^+$), and surrounding NC cells (Figure 6D,E). Thus, the PNPs showed stem cell-like behaviour by undergoing self-renewal and differentiating to form NC cells.

Modulation of TGF-β and SHH signalling locks in PNP rostrocaudal axis information

We have shown that the combined modulation of Wnt/FGF and RA signalling generated posterior PNPs. However, transcriptomics and lineage analysis indicated that PNP maintenance is compromised by NC bifurcations, the progressive activation of more posterior HOX genes, and late-passage differentiation/cell death. In an attempt to prevent this progressive posteriorisation and NC commitment, we supplemented our culture medium with modulators of other signalling pathways (Figure 7A). Inhibitors of Activin/Nodal (SB431542, SB) and BMP (LDN193189, LDN) signalling were used to supress EMT and NC specification (Cuny et al., 2008; Das, Becker, Hoffmann, & Mertz, 2009; Halder, Beauchamp, & Datta, 2005; Inman et al., 2002; K. F. Liem, Jr., Tremml, & Jessell, 1997; Stuhlmiller & Garcia-Castro, 2012). Furthermore, to mimic signals that arise from the notochord to ventralise neural progenitors during neural tube folding/cavitation, a smoothened agonist (SAG) was used to stimulate Sonic Hedgehog (SHH) signalling (Jessell, 2000; Sasai et al., 2014).

The combined addition of SB and LDN (+SBLDN) or SB and SAG (+SBSAG) at P3 resulted in stabilisation of PNPs for over 15 passages (60 days). At early passages (P5/P6), the addition of small molecules did not compromise the formation of $CDX2^+/SOX2^+$ PNPs, which organised into typical tightly associated colonies surrounded by loosely packed $SNAI1^+$ cells. (Figure 7B, Figure 7 - figure supplement 1A). However, both supplemented conditions modestly increased the percentage of $SOX2^+/CDX2^+$ cells as quantified by flow cytometry at later passages (P9/P10) (Figure 7C, Figure 7 - figure supplement 1B).

Cells maintained in +SBSAG and +SBLDN significantly prolonged *CDX2* and *SOX2* gene expression for up to 15 passages (Figure 7D). Moreover, based on the transcriptional profiling of *HOX* genes, the positional value of the PNPs was locked at the thoracic level, considerably slowing down the upregulation of terminal *HOXC13* and *HOXA1*3 (Figure 7E, Figure 7 - figure supplement 1C,D). Verrier et al. (2018) used the dual inhibition of Nodal/Activin and BMP signals to generate RA-induced neural progenitors from NMPs. However, these cells were not maintained over long time periods presumably because of their exposure to RA. In our tissue cultures, the RA target *PAX6* remained silent in +SBLDN or +SBSAG addition at P6/7 (Figure 7 - figure supplement 1E). These results therefore show that PNPs can be locked in a thoracic identity and grown in culture for long periods of time via the addition of TGF-β inhibitors to the media.

PNPs can give rise to spinal cord neurons

To establish whether these RA-deprived PNPs can generate neurons, we exposed them to a cocktail of terminal differentiation inducers for 12-24 days to cause them to terminally differentiate as neurons (Figure 8A). This resulted in neuronal cultures expressing the neuronal nuclei marker (NeuN), neuron-specific βIII-tubulin (TUJ) and SOX2 (Figure 8B). As expected, higher yields of $ISL1^+$ and $CHX10^+$ cells were noted in +SBSAG PNP-derived cultures, suggesting SHH signalling promotes the specification of motor neurons ($ISL1^+/TUJ^+$) or V2a interneurons ($CHX10^+/TUJ^+$) (Figure 8C) (Clovis et al., 2016; Le Dréau & Martí, 2012; Thaler, Lee, Jurata, Gill, & Pfaff, 2002). Together, these results show that PNPs grown with or without TGF-β inhibitors have the potential to generate neuronal derivatives and that PNP may be responsive to ventralising signals.

DISCUSSION

The NMP niche is maintained by Wnt/FGF-mediated autoregulatory loops, CYP26A1-mediated RA signal suppression, and active RARγ–mediated transcriptional repression (Abu-Abed et al., 2001; Cunningham, Kumar, Yamaguchi, & Duester, 2015; Deng et al., 1994; Amanda Janesick et al., 2014; Koide, Downes, Chandraratna, Blumberg, & Umesono, 2001; Liu et al., 1999; B. L. Martin & Kimelman, 2008; Benjamin L. Martin & Kimelman, 2010; Sakai et al., 2001; Takada et al., 1994; Takemoto, Uchikawa, Kamachi, & Kondoh, 2006; Yamaguchi, Takada, Yoshikawa, Wu, & McMahon, 1999). By simultaneously controlling these multiple signalling pathways *in vitro*, we have generated regionalised spinal cord progenitors and neural crest cells from hPSCs. Our protocol consistently yields a well-defined population of PNPs and NC cells characteristic of different positions along the rostrocaudal axis, providing a valuable source of spinal cord cells and neural crest which might be used for therapeutic applications, drug screening, or detailed disease modelling. In particular, we hope that

use of our protocol will improve our understanding of selective neuronal vulnerability, a recognised, yet poorly understood feature of neurodegenerative disease and spinal cord injury.

Previous studies show that *in vitro* generated NMPs, when passaged back into FGF/CHIR or CHIR alone, commit to a mesodermal lineage (Gouti et al., 2014; Turner et al., 2014). In contrast, we observed a gradual decrease in TBXT and TBX6 expression, and commitment of NMP-like cells to a neural trajectory. Interestingly, this appeared to occur independently of RA signalling. More recently, Edri *et al.*, (2019) found NMPs differentiated from mouse epiblast stem cells (EpiSCs), rather than ESCs, resemble more accurately their counterparts *in vivo* and have a similar progressive commitment to a neural fate after passaging (Edri et al., 2019). This is in line with our observations using hPSCs, and could reflect that hPSCs correspond more closely to the primed pluripotency state of mouse EpiSCs (Brons et al., 2007; Nichols & Smith, 2011). Compared to previous studies of *in vitro*-derived NMPs, the PNPs reported here are a more stable source of spinal cord as their maintenance does not depend on the delicate balance between TBXT and SOX2, and they do not express critical RA-responsive neurogenic genes like PAX6 and SOX1, which would promote their fate progression to spinal cord neurons (Gentsch, Monteiro, & Smith, 2017; A. Janesick, Wu, & Blumberg, 2015).

While PNPs were efficiently derived from NMPs, their long-term maintenance was accompanied by progressive posteriorisation and NC delamination. Thus, to promote PNP self-renewal, we tried to mimic the niche environment of axial stem cells by inhibiting TGFβ signalling and stimulating hedgehog signalling. TGFβ signal inhibition favoured PNP fate over time and locked progenitors in a thoracic HOX identity for over 15 passages, identifying the importance of TGFβ signal inhibition in PNT/PNP formation. Previous *in vivo* data supports this observation, as the inhibitory TGFβ signal transducer *SMAD6*, is specifically expressed in the PNT, while FST is required for dorsal-ventral patterning and neuronal fate specification in response to SHH signalling (K. F. Liem, Jessell, & Briscoe, 2000; Isabel Olivera-Martinez et al., 2014). Specifically, our data indicates Actvin/Nodal pathway inhibition may be sufficient to promote PNP identity in our culture, but perhaps acting to further enforce TGFβ superfamily inhibition which occurs at a low-level through FGF mediated repression of the BMP pathway (Furthauer, Van Celst, Thisse, & Thisse, 2004; Guo & Wang, 2009; Pera, Ikeda, Eivers, & De Robertis, 2003).

Our work also established that PNPs undergo EMT to form NC cells with corresponding rostrocaudal identity. Recent studies have shown that cranial NC is specified at the neural plate border and trunk NC arises from the NMP niche (Frith et al., 2018; Stuhlmiller & Garcia-Castro, 2012; Wymeersch et al., 2016). Concurrent with this idea, we demonstrated that NMP-derived PNPs have the potential to

generate trunk NC cells (Figure 9). Single PNPs gave rise to more PNPs ('self-renewal') and migratory NC cells indicating that trunk NC cells delaminate from the PNT (Frith et al., 2018; Gouti, Metzis, & Briscoe, 2015; Sasai et al., 2014). Here we are able to maintain PNPs which give rise to NC as they progress through a rostro to caudal identity. We did not observe any direct NC specification from NMPs. However, this remains a possibility which will be interesting to explore further.

ACKNOWLEDGEMENTS

We thank members of the following scientific platforms and units of the Francis Crick Institute for their expertise, support and use of the facilities: advanced sequencing facility, advanced light microscopy facility, the human embryo and stem cell unit, bioinformatics and biostatistics and research illustration and graphics. We also thank Rickie Patani, Jamie Mitchell, James Briscoe, Vicki Metzi, Teresa Rayon, Alessia Caramello, Robin Lovell-Badge, Siew-Lan Ang and Francois Guillemot for advice, help and reagents; Rebecca Jones and Clara Collart for critical reading of the manuscript; and the Smith lab for discussions and advice. This work was supported by the Francis Crick Institute which receives its core funding from Cancer Research UK (FC001-157), the UK Medical Research Council (FC001-157), and the Wellcome Trust (FC001-157) *and* a British Heart Foundation award (FS/12/37/29516). A.S.B. was supported by the British Heart Foundation (FS/12/37/29516) and is now supported by the Wellcome Trust (210987/Z/18/Z). J.C.S. was supported by the Medical Research Council (program number U117597140) and is now supported by the Francis Crick Institute, which receives its core funding from Cancer Research UK (FC001-157), the UK Medical Research Council (FC001-157), and the Wellcome Trust (FC001-157).

CONTRIBUTIONS

FC: Conceptualization, Validation, Conceptualization, Methodology, Investigation, Formal analysis, Writing—original draft, Supervision, Project administration

GEG: Conceptualization, Methodology, Investigation, Supervision, Project administration, Writing—review & editing

RM: Software, Methodology, Formal analysis, Writing—review & editing

CB: Investigation, Writing—review & editing

LH: Methodology, Investigation, Resources, Writing—review & editing

ARH: Investigation

JCS: Conceptualization, Writing—review & editing, Supervision, Funding acquisition

ASB: Conceptualization, Methodology, Investigation, Writing—review & editing, Supervision, Project administration, Funding acquisition

COMPETING INTERESTS

The authors have no competing interests to declare

METHODS

Human pluripotent stem cell culture

Human ESCs (WA09 and WA01, WiCell) and human iPSCs (AICS-23, Allen Institute) were maintained in feeder-free cultures, plated on Corning Matrigel Growth Factor Reduced (GFR) Basement Membrane Matrix (Corning Incorporated, 354230) and grown in mTESR1 (STEMCELL technologies, 85850). Cells were passaged as aggregates at a ratio of 1:10/15 using Gibco Versene Solution (Thermo Fisher Scientific, 15040066). All experiments were completed within 15 passages after recovery from cryopreservation and screened for mycoplasma monthly. Prior to cryopreservation, hPSCs were assessed for genetic stability by KaryoStat and indicators of pluripotency were assessed by PluriTest (Thermo Fisher Scientific). hPSCs were subject to routine pluripotency using BD Stemflow Human and Mouse Pluripotent Stem Cell Analysis Kit (BD Biosciences, 560477) as recommended by the manufacturers, or by immunostaining against OCT3/4, SOX2 and NANOG (see Table S5 for antibody details) using the standard immunostaining protocol below. All experiments with hESCs were approved by the UK Stem Cell Bank steering committee (SCSC13-03).

NMP differentiation

For differentiation into NMPs, confluent hPSCs were dissociated into single cells using Gibco TrypLE Express (Thermo Fisher Scientific, 12604013) and plated at a density of 50,000 cells/cm^2 on Matrigel hESC-Qualified Matrix (Corning Incorporated, 354277). Cells were plated in mTESR1 supplemented with 10 μM Y-27632 (Tocris, 1254) for a 24h to 36h to allow recovery before starting differentiation into NMPs. Following recovery time, cells were grown in Dulbecco's Modified Eagle Medium/Nutrient Mixture F-12 (DMEM/F-12, Thermo Fisher Scientific, 10565018) supplemented with 1x Gibco B-27 supplement minus vitamin A (Thermo Fisher Scientific, 12587010) and 1x Gibco N2 (Thermo Fisher Scientific, 17502048), 4-6 μM CHIR-99021 (Selleck Chem, S2924-SEL-5mg), 10 μM AGN193109 sodium salt (Santa Cruz, sc-210768) and 20 ng/ml FGF2 (R&D systems, 233-FB-025) referred to from now on as NMP differentiation medium. NMP differentiation medium was supplemented with and 5 μM Y-27632 (Tocris).

PNP long term culture

To generate PNPs, NMPs were passaged at 36h using TrypLE express (Thermo Fisher Scientific) and when confluent thereafter. Cells were passaged as single cells at a ratio of 1:6 into NMP differentiation medium, supplemented with 10 μM Y-27632 (Tocris). During passage 1 to 3 progenitors were found to detach from the dish forming spheres. If this occurred, spheres were dissociated into single cells and re-plated immediately. PNP generation was more successful if cells did not detach, therefore, to prevent cells

442 detaching during this period cells were passaged before reaching high confluency. In addition, cells were
443 only removed from the 37°C incubator when ready to passage, as the temperature fluctuations promoted
444 detachment. From passage 3 cells were grown NMP differentiation medium supplemented with 5 μM Y-
445 27632 (Tocris). Human iPSCs were found to detach more readily than hESCs. PNPs could be maintained, for
446 8 to 12 passages using standard conditions as above, passaging every 3-4 days when 80-90% confluent. To
447 lock A-P axis progression, 2 μM SB431542 (CELL guidance systems, SM33-10) and 100 nM LDN193189
448 (Sigma-Aldrich, SML0559-5MG) or SB431542 (CELL guidance systems, SM33-10) and 500nM smoothened
449 agonist (SAG, Sigma-Aldrich, 566660-1mg) were added to NMP differentiation medium at passage 3. For
450 selective detachment, 90% confluent PNPs were washed with PBS and treated with TrypLE express
451 (Thermo Fisher Scientific) at 37°C for 3-5 mins. When mesenchymal cells started to detach, cells were
452 gently removed by tilting the plate side-to-side. TrypLE containing the detached mesenchymal cells was
453 carefully removed. Remaining epithelial cells were washed off the vessel using basal medium.
454
455 **Neuronal differentiation**
456 To generate neurons, we used a modified protocol based on a previously published neural
457 differentiation protocol (Lippmann et al., 2015). 80-90% confluent PNP/NC cultures were dissociated
458 to single cells and plated at 1:20-1:30 onto Matrigel hESC-Qualified matrix (Corning) into the
459 applicable former culture medium (NMP differentiation medium plus or minus SB/LDN or SB/SAG).
460 24h after plating, medium was replaced with neural differentiation medium consisting of Gibco neural
461 basal medium (Thermo Fisher Scientific, 21103049) supplemented with Gibco 1x B-27 supplement
462 (Thermo Fisher Scientific, 17504044) and 1x N2 (Thermo Fisher Scientific), 2 μM DAPT (Chem Cruz, sc-
463 201315) and 10 ng/ml brain-derived neurotrophic factor (BDNF, PeproTech, 450-02-2UG), 10 ng/ml
464 glial-derived neurotrophic factor (GDNF, PeproTech, 450-10-2UG), 100 nM retinoic acid (RA, Sigma
465 Aldrich, sc-210768) and 1 mM cAMP (Sigma Aldrich, A6885-100mg) for 12-24 days. When 100%
466 confluent cells were passaged using TrypLE express and replated as single cells into neural
467 differentiation medium (as above) supplemented with 10 μM Y-27632 (Tocris) for the first 24h. During
468 neural induction and maintenance, growth medium was replaced every 48h.
469
470 **Neural crest differentiation**
471 To differentiate NC cells, 80-90% confluent PNP/NC cultures at P5 were dissociated to single cells and
472 plated at 1:10 onto Matrigel hESC-Qualified matrix (Corning) into DMEM:F12 (Thermo Fisher
473 Scientific) supplemented with 1x B27 supplement (Thermo Fisher Scientific) and 1% Fetal Bovine
474 Serum (FBS, Sigma Aldrich, F754) (Mohlin et al., 2019). Medium was replenished every 48h for 7 days.
475
476 **Immunofluorescence microscopy**

477 Cells were cultured in 8 or 12 well μ-slides (Ibidi) and fixed by adding ice-cold 4% Pierce formaldehyde
478 (w/v) methanol-free (Thermo Fisher Scientific, 28908) in PBS for 10-15 mins. Cells were permeabilised
479 in PBS supplemented with 0.1% (v/v) Triton-X100 (Sigma Aldrich, T8787-250ML) for 10 mins and then
480 blocked solution consisting of PBS supplemented with 0.1% (v/v) Triton-X100 (Sigma Aldrich), 5% (v/v)
481 Donkey serum (Merck Millipore, S30-100ML) for more than 1h at room temperature. Primary
482 antibodies were incubated in blocking solution at 4°C overnight in concentrations detailed in Table S6.
483 Cells were then washed in PBS and incubated in Donkey AlexaFluor conjugated secondary antibodies
484 (Abcam) diluted at 1:400 in blocking solution for more than 1 hour at room temperature. Cells were
485 mounted in Vectorshield antifade mounting medium containing DAPI (Vector Laboratories, H-1200-
486 10). Cells were imaged using two imaging systems; 1) by a Zeiss LSM710 confocal microscope (Carl
487 Ziess AG) using Zeiss Plan-Apochromat 20x/0.8 or 10x/0.45 objective (Carl Ziess AG) controlled by ZEN
488 Black 2012 software (Carl Ziess AG); and 2) by an inverted Olympus IX83 microscope (Olympus
489 Corporation) using an Olympus super-apochromatic 20x/0.75 objective (Olympus Corporation),
490 captured using a Hamamatsu Flash 4.0 sCMOS camera (Hamamatsu photonics), a Spectra X(LED) light-
491 source (Lumencore) and controlled by CellSens Dimension software (Olympus Corporation)). Post-
492 acquisition analysis was performed using (Fiji) Image J (Schindelin et al., 2012). Briefly, nuclear
493 segmentation was achieved using a fixed binary threshold using DAPI, the fluorescence intensity
494 (mean grey value) of each channel was masked back to nuclei.
495
496 **Flow Cytometry**
497 Cells were collected using Gibco TrypLE express (Thermo Fisher Scientific) dissociation, fixed by adding
498 ice-cold 4% Pierce formaldehyde (w/v) methanol-free (Thermo Fisher Scientific) in PBS for 15 mins,
499 and washed using PBS. Cells were permeabilised with PBS/0.5% Triton-X100 for 15m and blocked with
500 PBS supplemented with 0.1% (v/v) Triton-X100 (Sigma Aldrich), 1% BSA fraction V (w/v) (Sigma-
501 Aldrich, A3059) for 1hr while mixing on a slow speed gyratory motion shaker. Primary incubations
502 were completed in blocking buffer using Alexa Fluor 488 Mouse anti-SOX2 (BD Pharmingen, O30-678)
503 and Alexa Fluor® 647 Mouse anti-CDX-2 (BD Pharmingen, M39-711,). After washes, fluorescence was
504 immediately measured on a LSR II cytometer (BD Biosciences) and results were analysed using FlowJo
505 software (FlowJo LLC). Gates used to determine percentage of positive cells were designed based on
506 fluorescence levels detected in the control samples, which included both Alexa Fluor 488 Mouse IgG1
507 κ (MOPC-21, BD Pharmingen and Alexa Fluor 647 Mouse IgG1 κ (BD Pharmingen, MOPC-31C) isotype
508 control isotype and unstained sample. Aldehyde dehydrogenase activity was measured as per the
509 manufacturer's guidelines using the ALDEFLUOR Kit (STEMCELL Technologies, 01700). Fluorescence

was measured on a LSR II cytometer (BD Biosciences) and analysed using FlowJo software (FlowJo LLC).

Clonal expansion of PNPs and NC cells

To generate sub-clonal PNP and NC cell lines, passage 5 cells were selectively detached and dissociated into single cells using TrypLE express (Thermo Fisher Scientific) as previously described. Cells were resuspended into RPMI 1640 (Thermo Fisher Scientific, 32404-014) supplemented with 10% (v/v) KnockOut serum replacement, (KSR, Thermo Fisher Scientific, 10828028) and 10 μM Y-27632 (Tocris). Cells were sorted using a MoFlo XPD (Beckman Coulter) using FSC and SSC profile to select single, live cells. Cells were sorted into Matrigel hESC-Qualified Matrix (Corning) coated 96 well plates (Corning) containing NMP differentiation medium. Surviving cells were subsequently passaged TrypLE express (Thermo Fisher Scientific) to expand clonal population as previously described above.

RNA extraction, cDNA synthesis and qPCR

Total RNA extraction was completed using RNEasy mini kit (Qiagen, 74106) following the manufacturer's instructions. cDNA was synthesised using Maxima First Strand cDNA Synthesis Kit for RT-qPCR with dsDNase (Thermo Fisher Scientific, K1672) following manufacturer's instructions with the addition of a dilution step where cDNA was diluted 1:60 in water. qPCR analysis was performed using primers detailed in Table S5 on a Roche Lightcycler 480 II (Roche Holding AG) using LightCycler 480 SYBR Green I Master mix (Roche Holding AG, 04887352001). Relative expression was calculated using the ΔΔCt method, normalising each gene to porphobilinogen deaminase (PBGD) levels.

RNA-sequencing

RNA was extracted using RNEasy mini kit (Qiagen) following the manufacturer's instructions including recommended DNase digestion step. RNA concentration was measured on a on a GloMax (Promega Corporation) and RNA integrity on TapeStation (Agilent Technologies). Libraries were prepared using KAPA mRNA (PolyA) HyperPrep Kit (Roche Holding AG, KK8581) using 500 ng RNA per sample according to manufacturer's instructions. Libraries were sequenced using a HiSeq 4000 (Illumina Biotechnology) as follows: pooled to 4 nM, 75bp single end sequencing and up to 38 million reads per sample. Data is available at the GEO repository (accession number GSE150709).

RNA-seq analysis

Reads were Illumina adapter trimmed using Cutadapt v1.16 (M. Martin, 2011) and aligned against GRCh38 and Ensembl release 86 transcript annotations using STAR v2.5.2b (Dobin et al., 2013) via the

transcript quantification software RSEM v1.3.0 (B. Li & Dewey, 2011). Gene-level counts were rounded to integers and subsequently used for differential expression analysis with DESeq2 (Love et al., 2014). Differential expression analysis between pairwise replicate groups was thresholded for significance based on an FDR<=0.01, a fold-change of +/- 2, and a base-mean expression of >=100. PCA analysis was conducted on the normalised log transformed count data using the 10% most variable genes across samples. The volcano plot depicts the FDR and logFC statistics from the group DESeq2 differential expression analysis between P5 epithelial and P5 mesenchymal samples. For hierarchical clustering analysis, genes that maintained their significance and direction of change across 2 consecutive time-points were selected for visualisation in a heatmap. K-means clustering (k=10) was used to identify distinct gene clusters of related expression. Heatmaps show gene-level normalised counts, centred and scaled as z-scores. Gene ontology analysis was carried out using ToppGene Suite (ToppFun function) (Chen, Bardes, Aronow, & Jegga, 2009).

Comparison between data sets

Previously published Affymetrix array data were downloaded from the NCBI Gene Expression Omnibus (GEO) as GSE109267 (Frith et al., 2018). Cell files were imported into R and RMA processed using the Bioconductor package oligo with default settings. Differential expression analysis between NMP and hESC replicate groups was assessed using limma (Ritchie et al., 2015). Genes with an FDR corrected p-value <= 0.01 and fold change >= +/- 2 were called significant. NMP high genes from the Verrier et al (2018) study were provided in supplementary data and subsequently filtered using a P-value of <=0.01 (Verrier et al., 2018). The overlap between each genes list representing significantly upregulated genes at 36h was generated using BioVenn (Hulsen, de Vlieg, & Alkema, 2008). The overlap between each gene list was found to be significant (p<1e-4, hypergeometric distribution).

REFERENCES

Abu-Abed, S., Dollé, P., Metzger, D., Beckett, B., Chambon, P., & Petkovich, M. (2001). The retinoic acid-metabolizing enzyme, CYP26A1, is essential for normal hindbrain patterning, vertebral identity, and development of posterior structures. *Genes & development, 15*(2), 226-240. doi:10.1101/gad.855001

Aires, R., Jurberg, A. D., Leal, F., Nóvoa, A., Cohn, M. J., & Mallo, M. (2016). Oct4 Is a Key Regulator of Vertebrate Trunk Length Diversity. *Developmental Cell, 38*(3), 262-274. doi:https://doi.org/10.1016/j.devcel.2016.06.021

Amin, S., Neijts, R., Simmini, S., van Rooijen, C., Tan, S. C., Kester, L., . . . Deschamps, J. (2016). Cdx and T Brachyury Co-activate Growth Signaling in the Embryonic Axial Progenitor Niche. *Cell Rep, 17*(12), 3165-3177. doi:10.1016/j.celrep.2016.11.069

Brons, I. G., Smithers, L. E., Trotter, M. W., Rugg-Gunn, P., Sun, B., Chuva de Sousa Lopes, S. M., . . . Vallier, L. (2007). Derivation of pluripotent epiblast stem cells from mammalian embryos. *Nature, 448*(7150), 191-195. doi:10.1038/nature05950

Brown, J. M., & Storey, K. G. (2000). A region of the vertebrate neural plate in which neighbouring cells can adopt neural or epidermal fates. *Current Biology, 10*(14), 869-872. doi:https://doi.org/10.1016/S0960-9822(00)00601-1

Cajal, M., Lawson, K. A., Hill, B., Moreau, A., Rao, J., Ross, A., . . . Camus, A. (2012). Clonal and molecular analysis of the prospective anterior neural boundary in the mouse embryo. *Development, 139*(2), 423-436. doi:10.1242/dev.075499

Cambray, N., & Wilson, V. (2002). Axial progenitors with extensive potency are localised to the mouse chordoneural hinge. *Development, 129*(20), 4855.

Cambray, N., & Wilson, V. (2007). Two distinct sources for a population of maturing axial progenitors. *Development, 134*(15), 2829. doi:10.1242/dev.02877

Cano, A., Perez-Moreno, M. A., Rodrigo, I., Locascio, A., Blanco, M. J., del Barrio, M. G., . . . Nieto, M. A. (2000). The transcription factor snail controls epithelial-mesenchymal transitions by repressing E-cadherin expression. *Nat Cell Biol, 2*(2), 76-83. doi:10.1038/35000025

Chambers, S. M., Fasano, C. A., Papapetrou, E. P., Tomishima, M., Sadelain, M., & Studer, L. (2009). Highly efficient neural conversion of human ES and iPS cells by dual inhibition of SMAD signaling. *Nat Biotechnol, 27*(3), 275-280. doi:10.1038/nbt.1529

Chen, J., Bardes, E. E., Aronow, B. J., & Jegga, A. G. (2009). ToppGene Suite for gene list enrichment analysis and candidate gene prioritization. *Nucleic Acids Res, 37*(Web Server issue), W305-311. doi:10.1093/nar/gkp427

Clovis, Y. M., Seo, S. Y., Kwon, J.-s., Rhee, J. C., Yeo, S., Lee, J. W., . . . Lee, S.-K. (2016). Chx10 Consolidates V2a Interneuron Identity through Two Distinct Gene Repression Modes. *Cell Reports, 16*(6), 1642-1652. doi:https://doi.org/10.1016/j.celrep.2016.06.100

Cunningham, T. J., Kumar, S., Yamaguchi, T. P., & Duester, G. (2015). Wnt8a and Wnt3a cooperate in the axial stem cell niche to promote mammalian body axis extension. *Developmental dynamics : an official publication of the American Association of Anatomists, 244*(6), 797-807. doi:10.1002/dvdy.24275

Cuny, G. D., Yu, P. B., Laha, J. K., Xing, X., Liu, J.-F., Lai, C. S., . . . Peterson, R. T. (2008). Structure-activity relationship study of bone morphogenetic protein (BMP) signaling inhibitors. *Bioorganic & medicinal chemistry letters, 18*(15), 4388-4392. doi:10.1016/j.bmcl.2008.06.052

Das, S., Becker, B. N., Hoffmann, F. M., & Mertz, J. E. (2009). Complete reversal of epithelial to mesenchymal transition requires inhibition of both ZEB expression and the Rho pathway. *BMC cell biology, 10*, 94-94. doi:10.1186/1471-2121-10-94

Delfino-Machin, M., Lunn, J. S., Breitkreuz, D. N., Akai, J., & Storey, K. G. (2005). Specification and maintenance of the spinal cord stem zone. *Development, 132*(19), 4273-4283. doi:10.1242/dev.02009

Denans, N., Iimura, T., & Pourquie, O. (2015). Hox genes control vertebrate body elongation by collinear Wnt repression. *Elife, 4*. doi:10.7554/eLife.04379

Deng, C. X., Wynshaw-Boris, A., Shen, M. M., Daugherty, C., Ornitz, D. M., & Leder, P. (1994). Murine FGFR-1 is required for early postimplantation growth and axial organization. *Genes & development, 8*(24), 3045-3057. doi:10.1101/gad.8.24.3045

Denham, M., Hasegawa, K., Menheniott, T., Rollo, B., Zhang, D., Hough, S., . . . Dottori, M. (2015). Multipotent Caudal Neural Progenitors Derived from Human Pluripotent Stem Cells That Give Rise to Lineages of the Central and Peripheral Nervous System. *STEM CELLS, 33*(6), 1759-1770. doi:10.1002/stem.1991

Diez del Corral, R., Breitkreuz, D. N., & Storey, K. G. (2002). Onset of neuronal differentiation is regulated by paraxial mesoderm and requires attenuation of FGF signalling. *Development, 129*(7), 1681.

Diez del Corral, R., Olivera-Martinez, I., Goriely, A., Gale, E., Maden, M., & Storey, K. (2003). Opposing FGF and retinoid pathways control ventral neural pattern, neuronal differentiation, and segmentation during body axis extension. *Neuron, 40*(1), 65-79. doi:10.1016/s0896-6273(03)00565-8

Dobin, A., Davis, C. A., Schlesinger, F., Drenkow, J., Zaleski, C., Jha, S., . . . Gingeras, T. R. (2013). STAR: ultrafast universal RNA-seq aligner. *Bioinformatics, 29*(1), 15-21. doi:10.1093/bioinformatics/bts635

Edri, S., Hayward, P., Baillie-Johnson, P., Steventon, B. J., & Martinez Arias, A. (2019). An epiblast stem cell-derived multipotent progenitor population for axial extension. *Development, 146*(10), dev168187. doi:10.1242/dev.168187

Frith, T. J., Granata, I., Wind, M., Stout, E., Thompson, O., Neumann, K., . . . Tsakiridis, A. (2018). Human axial progenitors generate trunk neural crest cells in vitro. *Elife, 7*. doi:10.7554/eLife.35786

Furthauer, M., Van Celst, J., Thisse, C., & Thisse, B. (2004). Fgf signalling controls the dorsoventral patterning of the zebrafish embryo. *Development, 131*(12), 2853-2864. doi:10.1242/dev.01156

Gentsch, G. E., Monteiro, R. S., & Smith, J. C. (2017). Cooperation Between T-Box Factors Regulates the Continuous Segregation of Germ Layers During Vertebrate Embryogenesis. *Curr Top Dev Biol, 122*, 117-159. doi:10.1016/bs.ctdb.2016.07.012

Gomez, G. A., Prasad, M. S., Wong, M., Charney, R. M., Shelar, P. B., Sandhu, N., . . . Garcia-Castro, M. I. (2019). WNT/beta-catenin modulates the axial identity of embryonic stem cell-derived human neural crest. *Development, 146*(16). doi:10.1242/dev.175604

Gouti, M., Delile, J., Stamataki, D., Wymeersch, F. J., Huang, Y., Kleinjung, J., . . . Briscoe, J. (2017). A Gene Regulatory Network Balances Neural and Mesoderm Specification during Vertebrate Trunk Development. *Dev Cell, 41*(3), 243-261 e247. doi:10.1016/j.devcel.2017.04.002

Gouti, M., Metzis, V., & Briscoe, J. (2015). The route to spinal cord cell types: a tale of signals and switches. *Trends Genet, 31*(6), 282-289. doi:10.1016/j.tig.2015.03.001

Gouti, M., Tsakiridis, A., Wymeersch, F. J., Huang, Y., Kleinjung, J., Wilson, V., & Briscoe, J. (2014). In vitro generation of neuromesodermal progenitors reveals distinct roles for wnt signalling in the specification of spinal cord and paraxial mesoderm identity. *PLoS Biol, 12*(8), e1001937. doi:10.1371/journal.pbio.1001937

Guo, X., & Wang, X.-F. (2009). Signaling cross-talk between TGF-β/BMP and other pathways. *Cell Research, 19*(1), 71-88. doi:10.1038/cr.2008.302

Hackland, J. O. S., Shelar, P. B., Sandhu, N., Prasad, M. S., Charney, R. M., Gomez, G. A., . . . Garcia-Castro, M. I. (2019). FGF Modulates the Axial Identity of Trunk hPSC-Derived Neural Crest but Not the Cranial-Trunk Decision. *Stem cell reports, 12*(5), 920-933. doi:10.1016/j.stemcr.2019.04.015

Halder, S. K., Beauchamp, R. D., & Datta, P. K. (2005). A specific inhibitor of TGF-beta receptor kinase, SB-431542, as a potent antitumor agent for human cancers. *Neoplasia (New York, N.Y.), 7*(5), 509-521. doi:10.1593/neo.04640

Henrique, D., Abranches, E., Verrier, L., & Storey, K. G. (2015). Neuromesodermal progenitors and the making of the spinal cord. *Development, 142*(17), 2864-2875. doi:10.1242/dev.119768

Hulsen, T., de Vlieg, J., & Alkema, W. (2008). BioVenn - a web application for the comparison and visualization of biological lists using area-proportional Venn diagrams. *BMC Genomics, 9*, 488. doi:10.1186/1471-2164-9-488

Inman, G. J., Nicolas, F. J., Callahan, J. F., Harling, J. D., Gaster, L. M., Reith, A. D., . . . Hill, C. S. (2002). SB-431542 is a potent and specific inhibitor of transforming growth factor-beta superfamily type I activin receptor-like kinase (ALK) receptors ALK4, ALK5, and ALK7. *Mol Pharmacol, 62*(1), 65-74. doi:10.1124/mol.62.1.65

Janesick, A., Nguyen, T. T. L., Aisaki, K.-i., Igarashi, K., Kitajima, S., Chandraratna, R. A. S., . . . Blumberg, B. (2014). Active repression by RARγ signaling is required for vertebrate axial elongation. *Development, 141*(11), 2260. doi:10.1242/dev.103705

Janesick, A., Wu, S. C., & Blumberg, B. (2015). Retinoic acid signaling and neuronal differentiation. *Cell Mol Life Sci, 72*(8), 1559-1576. doi:10.1007/s00018-014-1815-9

Javali, A., Misra, A., Leonavicius, K., Acharyya, D., Vyas, B., & Sambasivan, R. (2017). Co-expression of Tbx6 and Sox2 identifies a novel transient neuromesoderm progenitor cell state. *Development, 144*(24), 4522-4529. doi:10.1242/dev.153262

Jessell, T. M. (2000). Neuronal specification in the spinal cord: inductive signals and transcriptional codes. *Nat Rev Genet, 1*(1), 20-29. doi:10.1038/35049541

Kadoya, K., Lu, P., Nguyen, K., Lee-Kubli, C., Kumamaru, H., Yao, L., . . . Tuszynski, M. H. (2016). Spinal cord reconstitution with homologous neural grafts enables robust corticospinal regeneration. *Nature medicine, 22*(5), 479-487. doi:10.1038/nm.4066

Klein, E. S., Pino, M. E., Johnson, A. T., Davies, P. J., Nagpal, S., Thacher, S. M., . . . Chandraratna, R. A. (1996). Identification and functional separation of retinoic acid receptor neutral antagonists and inverse agonists. *J Biol Chem, 271*(37), 22692-22696. doi:10.1074/jbc.271.37.22692

Koch, F., Scholze, M., Wittler, L., Schifferl, D., Sudheer, S., Grote, P., . . . Herrmann, B. G. (2017). Antagonistic Activities of Sox2 and Brachyury Control the Fate Choice of Neuro-Mesodermal Progenitors. *Dev Cell, 42*(5), 514-526 e517. doi:10.1016/j.devcel.2017.07.021

Koide, T., Downes, M., Chandraratna, R. A., Blumberg, B., & Umesono, K. (2001). Active repression of RAR signaling is required for head formation. *Genes & development, 15*(16), 2111-2121. doi:10.1101/gad.908801

Kumamaru, H., Kadoya, K., Adler, A. F., Takashima, Y., Graham, L., Coppola, G., & Tuszynski, M. H. (2018). Generation and post-injury integration of human spinal cord neural stem cells. *Nat Methods, 15*(9), 723-731. doi:10.1038/s41592-018-0074-3

Le Dréau, G., & Martí, E. (2012). Dorsal–ventral patterning of the neural tube: A tale of three signals. *Developmental Neurobiology, 72*(12), 1471-1481. doi:10.1002/dneu.22015

Lee, H., Shamy, G. A., Elkabetz, Y., Schofield, C. M., Harrsion, N. L., Panagiotakos, G., . . . Studer, L. (2007). Directed differentiation and transplantation of human embryonic stem cell-derived motoneurons. *STEM CELLS, 25*(8), 1931-1939. doi:10.1634/stemcells.2007-0097

Leung, A. W., Murdoch, B., Salem, A. F., Prasad, M. S., Gomez, G. A., & Garcia-Castro, M. I. (2016). WNT/beta-catenin signaling mediates human neural crest induction via a pre-neural border intermediate. *Development, 143*(3), 398-410. doi:10.1242/dev.130849

Li, B., & Dewey, C. N. (2011). RSEM: accurate transcript quantification from RNA-Seq data with or without a reference genome. *BMC Bioinformatics, 12*, 323. doi:10.1186/1471-2105-12-323

Li, X., Liu, Z., Qiu, M., & Yang, Z. (2014). Sp8 plays a supplementary role to Pax6 in establishing the pMN/p3 domain boundary in the spinal cord. *Development, 141*(14), 2875-2884. doi:10.1242/dev.105387

Li, X. J., Du, Z. W., Zarnowska, E. D., Pankratz, M., Hansen, L. O., Pearce, R. A., & Zhang, S. C. (2005). Specification of motoneurons from human embryonic stem cells. *Nat Biotechnol, 23*(2), 215-221. doi:10.1038/nbt1063

Liem, K. F., Jessell, T. M., & Briscoe, J. (2000). Regulation of the neural patterning activity of sonic hedgehog by secreted BMP inhibitors expressed by notochord and somites. *Development, 127*(22), 4855.

Liem, K. F., Jr., Tremml, G., & Jessell, T. M. (1997). A role for the roof plate and its resident TGFbeta-related proteins in neuronal patterning in the dorsal spinal cord. *Cell, 91*(1), 127-138. doi:10.1016/s0092-8674(01)80015-5

Lippmann, E. S., Williams, C. E., Ruhl, D. A., Estevez-Silva, M. C., Chapman, E. R., Coon, J. J., & Ashton, R. S. (2015). Deterministic HOX patterning in human pluripotent stem cell-derived neuroectoderm. *Stem cell reports, 4*(4), 632-644. doi:10.1016/j.stemcr.2015.02.018

Liu, P., Wakamiya, M., Shea, M. J., Albrecht, U., Behringer, R. R., & Bradley, A. (1999). Requirement for Wnt3 in vertebrate axis formation. *Nat Genet, 22*(4), 361-365. doi:10.1038/11932

Lunn, J. S., Fishwick, K. J., Halley, P. A., & Storey, K. G. (2007). A spatial and temporal map of FGF/Erk1/2 activity and response repertoires in the early chick embryo. *Dev Biol, 302*(2), 536-552. doi:10.1016/j.ydbio.2006.10.014

Luu, B., Ellisor, D., & Zervas, M. (2011). The Lineage Contribution and Role of Gbx2 in Spinal Cord Development. *PLoS One, 6*(6), e20940. doi:10.1371/journal.pone.0020940

Martin, B. L., & Kimelman, D. (2008). Regulation of canonical Wnt signaling by Brachyury is essential for posterior mesoderm formation. *Dev Cell, 15*(1), 121-133. doi:10.1016/j.devcel.2008.04.013

Martin, B. L., & Kimelman, D. (2010). Brachyury establishes the embryonic mesodermal progenitor niche. *Genes & development, 24*(24), 2778-2783. doi:10.1101/gad.1962910

Martin, M. (2011). Cutadapt removes adapter sequences from high-throughput sequencing reads. *EMBnet.journal; Vol 17, No 1: Next Generation Sequencing Data AnalysisDO - 10.14806/ej.17.1.200*.

Mathis, L., & Nicolas, J. F. (2000). Different clonal dispersion in the rostral and caudal mouse central nervous system. *Development, 127*(6), 1277.

Mazzoni, E. O., Mahony, S., Peljto, M., Patel, T., Thornton, S. R., McCuine, S., . . . Wichterle, H. (2013). Saltatory remodeling of Hox chromatin in response to rostrocaudal patterning signals. *Nat Neurosci, 16*(9), 1191-1198. doi:10.1038/nn.3490

Mohlin, S., Kunttas, E., Persson, C. U., Abdel-Haq, R., Castillo, A., Murko, C., . . . Kerosuo, L. (2019). Maintaining multipotent trunk neural crest stem cells as self-renewing crestospheres. *Dev Biol, 447*(2), 137-146. doi:10.1016/j.ydbio.2019.01.010

Nagoshi, N., Tsuji, O., Nakamura, M., & Okano, H. (2019). Cell therapy for spinal cord injury using induced pluripotent stem cells. *Regenerative therapy, 11*, 75-80. doi:10.1016/j.reth.2019.05.006

Neijts, R., Amin, S., van Rooijen, C., & Deschamps, J. (2017). Cdx is crucial for the timing mechanism driving colinear Hox activation and defines a trunk segment in the Hox cluster topology. *Dev Biol, 422*(2), 146-154. doi:10.1016/j.ydbio.2016.12.024

Nichols, J., & Smith, A. (2011). The origin and identity of embryonic stem cells. *Development, 138*(1), 3. doi:10.1242/dev.050831

Nijssen, J., Comley, L. H., & Hedlund, E. (2017). Motor neuron vulnerability and resistance in amyotrophic lateral sclerosis. *Acta neuropathologica, 133*(6), 863-885. doi:10.1007/s00401-017-1708-8

Olivera-Martinez, I., Schurch, N., Li, R. A., Song, J., Halley, P. A., Das, R. M., . . . Storey, K. G. (2014). Major transcriptome re-organisation and abrupt changes in signalling, cell cycle and chromatin regulation at neural differentiation in vivo. *Development, 141*(16), 3266-3276. doi:10.1242/dev.112623

Olivera-Martinez, I., & Storey, K. G. (2007). Wnt signals provide a timing mechanism for the FGF-retinoid differentiation switch during vertebrate body axis extension. *Development, 134*(11), 2125-2135. doi:10.1242/dev.000216

Peljto, M., Dasen, J. S., Mazzoni, E. O., Jessell, T. M., & Wichterle, H. (2010). Functional diversity of ESC-derived motor neuron subtypes revealed through intraspinal transplantation. *Cell Stem Cell, 7*(3), 355-366. doi:10.1016/j.stem.2010.07.013

Pera, E. M., Ikeda, A., Eivers, E., & De Robertis, E. M. (2003). Integration of IGF, FGF, and anti-BMP signals via Smad1 phosphorylation in neural induction. *Genes & development, 17*(24), 3023-3028. doi:10.1101/gad.1153603

Philippidou, P., & Dasen, J. S. (2013). Hox genes: choreographers in neural development, architects of circuit organization. *Neuron, 80*(1), 12-34. doi:10.1016/j.neuron.2013.09.020

Ribes, V., Stutzmann, F., Bianchetti, L., Guillemot, F., Dollé, P., & Le Roux, I. (2008). Combinatorial signalling controls Neurogenin2 expression at the onset of spinal neurogenesis. *Developmental Biology, 321*(2), 470-481. doi:https://doi.org/10.1016/j.ydbio.2008.06.003

Ritchie, M. E., Phipson, B., Wu, D., Hu, Y., Law, C. W., Shi, W., & Smyth, G. K. (2015). limma powers differential expression analyses for RNA-sequencing and microarray studies. *Nucleic Acids Res, 43*(7), e47. doi:10.1093/nar/gkv007

Sakai, Y., Meno, C., Fujii, H., Nishino, J., Shiratori, H., Saijoh, Y., . . . Hamada, H. (2001). The retinoic acid-inactivating enzyme CYP26 is essential for establishing an uneven

distribution of retinoic acid along the anterio-posterior axis within the mouse embryo. *Genes & development, 15*(2), 213-225. doi:10.1101/gad.851501

Sandberg, M., Kallstrom, M., & Muhr, J. (2005). Sox21 promotes the progression of vertebrate neurogenesis. *Nat Neurosci, 8*(8), 995-1001. doi:10.1038/nn1493

Sasai, N., Kutejova, E., & Briscoe, J. (2014). Integration of signals along orthogonal axes of the vertebrate neural tube controls progenitor competence and increases cell diversity. *PLoS Biol, 12*(7), e1001907. doi:10.1371/journal.pbio.1001907

Schindelin, J., Arganda-Carreras, I., Frise, E., Kaynig, V., Longair, M., Pietzsch, T., . . . Cardona, A. (2012). Fiji: an open-source platform for biological-image analysis. *Nature Methods, 9*(7), 676-682. doi:10.1038/nmeth.2019

Shum, A. S., Poon, L. L., Tang, W. W., Koide, T., Chan, B. W., Leung, Y. C., . . . Copp, A. J. (1999). Retinoic acid induces down-regulation of Wnt-3a, apoptosis and diversion of tail bud cells to a neural fate in the mouse embryo. *Mech Dev, 84*(1-2), 17-30. doi:10.1016/s0925-4773(99)00059-3

Simoes-Costa, M., & Bronner, M. E. (2015). Establishing neural crest identity: a gene regulatory recipe. *Development, 142*(2), 242-257. doi:10.1242/dev.105445

Snyder, E. Y. (2017). The state of the art in stem cell biology and regenerative medicine: the end of the beginning. *Pediatric Research, 83*(1-2), 191-204. doi:10.1038/pr.2017.258

Storey, K. G., Goriely, A., Sargent, C. M., Brown, J. M., Burns, H. D., Abud, H. M., & Heath, J. K. (1998). Early posterior neural tissue is induced by FGF in the chick embryo. *Development, 125*(3), 473.

Stuhlmiller, T. J., & Garcia-Castro, M. I. (2012). Current perspectives of the signaling pathways directing neural crest induction. *Cell Mol Life Sci, 69*(22), 3715-3737. doi:10.1007/s00018-012-0991-8

Takada, S., Stark, K. L., Shea, M. J., Vassileva, G., McMahon, J. A., & McMahon, A. P. (1994). Wnt-3a regulates somite and tailbud formation in the mouse embryo. *Genes & development, 8*(2), 174-189. doi:10.1101/gad.8.2.174

Takemoto, T., Uchikawa, M., Kamachi, Y., & Kondoh, H. (2006). Convergence of Wnt and FGF signals in the genesis of posterior neural plate through activation of the Sox2 enhancer N-1. *Development, 133*(2), 297-306. doi:10.1242/dev.02196

Takemoto, T., Uchikawa, M., Yoshida, M., Bell, D. M., Lovell-Badge, R., Papaioannou, V. E., & Kondoh, H. (2011). Tbx6-dependent Sox2 regulation determines neural or mesodermal fate in axial stem cells. *Nature, 470*(7334), 394-398. doi:10.1038/nature09729

Thaler, J. P., Lee, S.-K., Jurata, L. W., Gill, G. N., & Pfaff, S. L. (2002). LIM Factor Lhx3 Contributes to the Specification of Motor Neuron and Interneuron Identity through Cell-Type-Specific Protein-Protein Interactions. *Cell, 110*(2), 237-249. doi:10.1016/S0092-8674(02)00823-1

Trawczynski, M., Liu, G., David, B. T., & Fessler, R. G. (2019). Restoring Motor Neurons in Spinal Cord Injury With Induced Pluripotent Stem Cells. *Front Cell Neurosci, 13*, 369. doi:10.3389/fncel.2019.00369

Tsakiridis, A., Huang, Y., Blin, G., Skylaki, S., Wymeersch, F., Osorno, R., . . . Wilson, V. (2014). Distinct Wnt-driven primitive streak-like populations reflect in vivo lineage precursors. *Development, 141*(6), 1209-1221. doi:10.1242/dev.101014

Turner, D. A., Hayward, P. C., Baillie-Johnson, P., Rue, P., Broome, R., Faunes, F., & Martinez Arias, A. (2014). Wnt/beta-catenin and FGF signalling direct the specification and

maintenance of a neuromesodermal axial progenitor in ensembles of mouse embryonic stem cells. *Development, 141*(22), 4243-4253. doi:10.1242/dev.112979

Tzouanacou, E., Wegener, A., Wymeersch, F. J., Wilson, V., & Nicolas, J. F. (2009). Redefining the progression of lineage segregations during mammalian embryogenesis by clonal analysis. *Dev Cell, 17*(3), 365-376. doi:10.1016/j.devcel.2009.08.002

van de Ven, C., Bialecka, M., Neijts, R., Young, T., Rowland, J. E., Stringer, E. J., . . . Deschamps, J. (2011). Concerted involvement of Cdx/Hox genes and Wnt signaling in morphogenesis of the caudal neural tube and cloacal derivatives from the posterior growth zone. *Development, 138*(16), 3451-3462. doi:10.1242/dev.066118

van den Akker, E., Forlani, S., Chawengsaksophak, K., de Graaff, W., Beck, F., Meyer, B. I., & Deschamps, J. (2002). Cdx1 and Cdx2 have overlapping functions in anteroposterior patterning and posterior axis elongation. *Development, 129*(9), 2181.

Verrier, L., Davidson, L., Gierlinski, M., Dady, A., & Storey, K. G. (2018). Neural differentiation, selection and transcriptomic profiling of human neuromesodermal progenitor-like cells in vitro. *Development, 145*(16). doi:10.1242/dev.166215

Wang, H., Li, D., Zhai, Z., Zhang, X., Huang, W., Chen, X., . . . Li, W. (2019). Characterization and Therapeutic Application of Mesenchymal Stem Cells with Neuromesodermal Origin from Human Pluripotent Stem Cells. *Theranostics, 9*(6), 1683-1697. doi:10.7150/thno.30487

Wichterle, H., Lieberam, I., Porter, J. A., & Jessell, T. M. (2002). Directed Differentiation of Embryonic Stem Cells into Motor Neurons. *Cell, 110*(3), 385-397. doi:https://doi.org/10.1016/S0092-8674(02)00835-8

Wilson, V., Olivera-Martinez, I., & Storey, K. G. (2009). Stem cells, signals and vertebrate body axis extension. *Development, 136*(10), 1591-1604. doi:10.1242/dev.021246

Wymeersch, F. J., Huang, Y., Blin, G., Cambray, N., Wilkie, R., Wong, F. C., & Wilson, V. (2016). Position-dependent plasticity of distinct progenitor types in the primitive streak. *Elife, 5*, e10042. doi:10.7554/eLife.10042

Yamaguchi, T. P., Takada, S., Yoshikawa, Y., Wu, N., & McMahon, A. P. (1999). T (Brachyury) is a direct target of Wnt3a during paraxial mesoderm specification. *Genes & development, 13*(24), 3185-3190. doi:10.1101/gad.13.24.3185

894 **FIGURES**

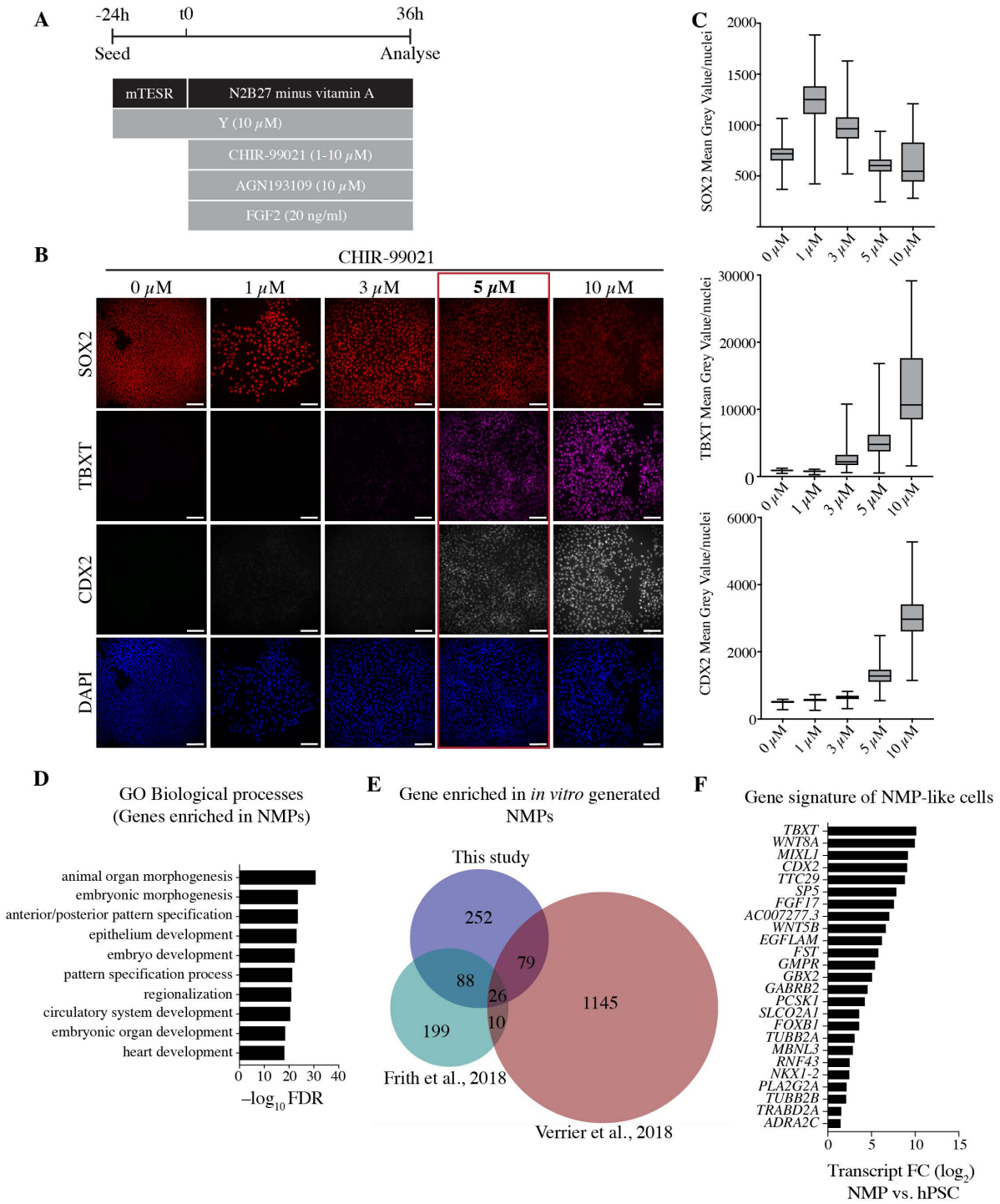

895 **Figure 1: NMP-like cells are induced by intermediate Wnt signalling in the presence of FGF and**
896 **inhibited RA signalling.**

897 A) Tissue culture scheme for optimising NMP generation from hPSCs. hPSCs are plated 24h before
898 exposure to FGF2 (20ng/ml), CHIR-99021 (0-10 µM), AGN193109 (10 µM) and Y-27632 (10 µM) for
899 36h. B) Representative immunostaining of 36h cultures treated as shown in (A), showing characteristic
900 NMP markers SOX2 (red), TBXT (magenta), CDX2 (grey) and the nuclear stain DAPI (blue) under

different CHIR-99021 concentrations. Scale bars, 100 µm. C) Box-plots showing mean grey value/nuclei quantified from repeat experiments as shown in (B). Each plot show data points collected from 2-4 experiments (>200 nuclei). D) Biological process GO analysis for genes significantly upregulated in NMPs compared to pluripotent hESCs. The top 10 biological process terms with the corresponding Benjamini and Hochberg adjusted p-values (FDR) are shown. E) Venn diagram showing the overlap of significantly upregulated genes in NMPs as reported in this study, Frith et al., (2018) and Verrier et al., (2018). F) Graph showing transcriptional fold change (FC) within the dataset of this study, of 26 genes commonly upregulated in NMPs according to Venn diagram in (E).

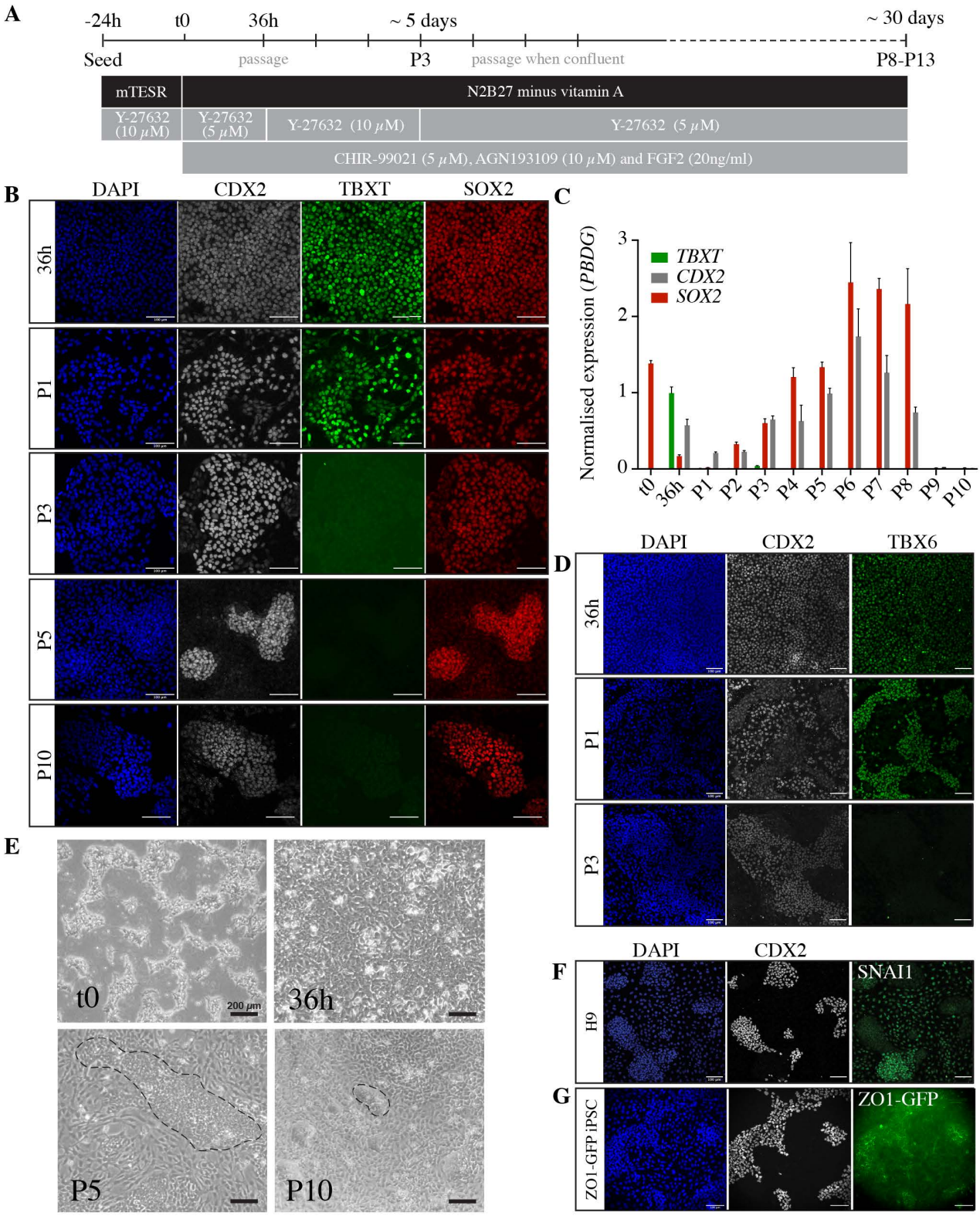

Figure 2: Long term culture of NMPs in the presence of Wnt/FGF and inhibited RA signalling generates epithelial SOX2⁺/CDX2⁺ cell colonies.

A) Tissue culture scheme for generating NMPs and maintaining neural progenitors *in vitro*. Cells are passaged at 36h and subsequently passaged at 80-90% confluency for up to 13 passages in FGF2 (20ng/ml), CHIR-99021 (5 µM), AGN193109 (10 µM) and Y-27632 (10 or 5 µM). B) Representative

immunostaining of CDX2 (grey), TBXT (magenta), SOX2 (red) and nuclear stain DAPI (blue) at increasing stages of tissue culture (36h, passage (P)1, P3, P5 and P10). Scale bars, 100 µm. C) Transcriptional analysis (RT-qPCR) of NMP markers at each passage up to passage 10. Expression levels are normalised to the reference gene *PBDG*. Error bars show SD, (n=3 technical replicates). Data are representative of three independent experiments, biological replicates provided in Figure 2 - figure supplement 1A,B. D) Representative immunostaining of TBX6 (green), CDX2 (grey) and nuclear stain DAPI (blue) at 36h, P1 and P3. Scale bar, 100 µm. E) Representative brightfield images of cells at the indicated stages. Dashed lines in P5 and P10 outline examples of a compact epithelial colonies, which are surrounded by flat mesenchymal cells. Scale bar, 200 µm. F) Representative immunostaining of CDX2 (grey), SNAI1 (green) and the nuclear stain DAPI (blue) at passage 5. Scale bar, 100 µm. G) Representative immunostaining of CDX2 (grey), GFP (ZO1-mEGFP iPSC, green) and the nuclear stain DAPI (blue) at passage 5. Scale bar, 100 µm.

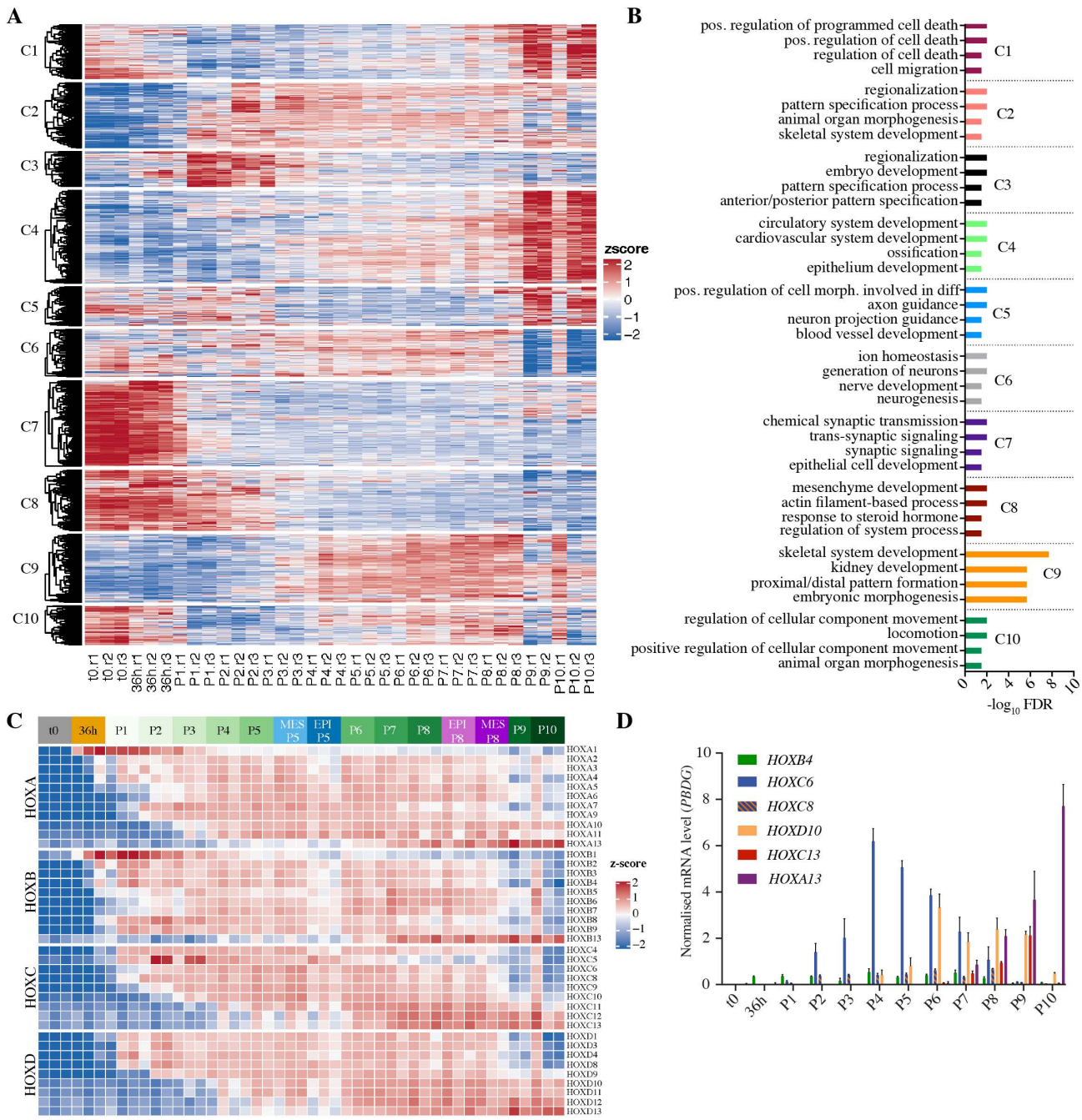

Figure 3: RNA-Seq analysis indicates NMPs transition to neural progenitors and neural crest derivatives.

A) Heatmap showing dynamically expressed genes (z-score) sorted into 10 clusters (C1-10) using k-means hierarchical clustering. Each cluster represents a different temporal expression pattern. B) Biological processes GO analysis for gene sets in each cluster shown in (A). The corresponding Benjamini and Hochberg adjusted p-values (FDR) are shown. C) Heatmap of expressed *HOX(A-D)* genes (z-score) across each time point including enriched epithelial (EPI) and mesenchymal (MES) samples at P5 and P8. D) Transcript levels of selected *HOX* genes as measured by RT-qPCR. Expression level was normalised to the reference gene *PBGD*. Error bars show SD, (n=3 technical replicates). Data are representative of three independent experiments, replicates provided in Figure 3 - figure supplement 2A,B.

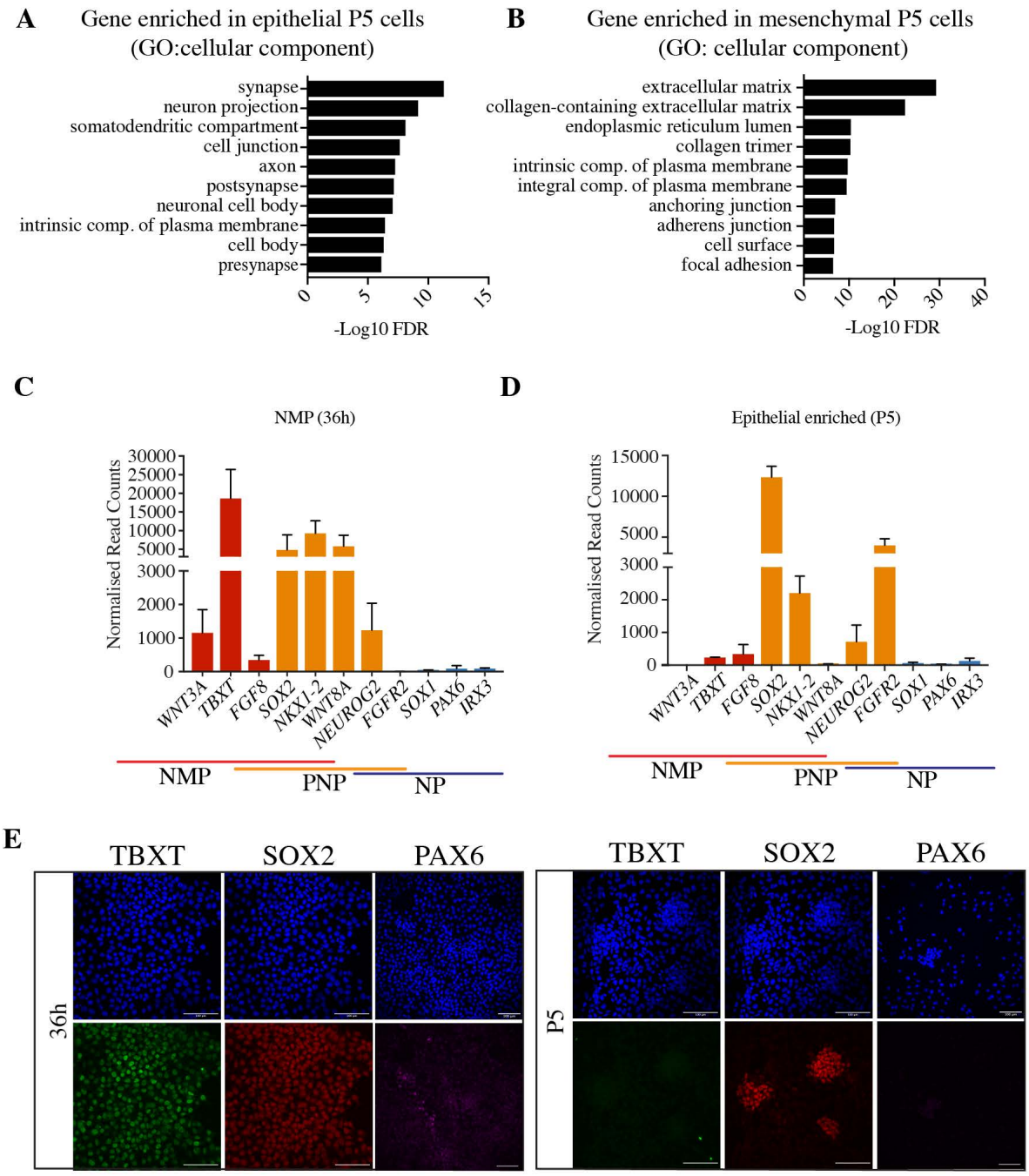

Figure 4: NMP-derived cells stabilise as epithelial pre-neural progenitors.

A,B) Graphs showing cellular component GO analysis for differentially expressed genes in P5 epithelial samples (A) and P5 mesenchymal samples (B). The corresponding Benjamini and Hochberg adjusted p-values (FDR) are shown. C, D) Normalised expression levels of known markers of NMPs (*WNT3A*, *TBXT*, *FGF8*, *SOX2*, *NKX1-2* and *WNT8A/C*), PNPs (*SOX2*, *NKX1-2*, *WNT8A/C, NEUROG2 and FGFR2*) and NPs (*PAX6*, IRX3, FGFR2, *NEUROG2* and *SOX1*) at 36h (C) and in P5 epithelial colonies (D) as determined by RNA-seq. Error bars show SEM (n = 3 biological replicates). E) Representative immunostaining of TBXT (green), SOX2 (red) and PAX6 (magenta) confirming the expression patterns shown in (A and B). Scale bars, 100 µm.

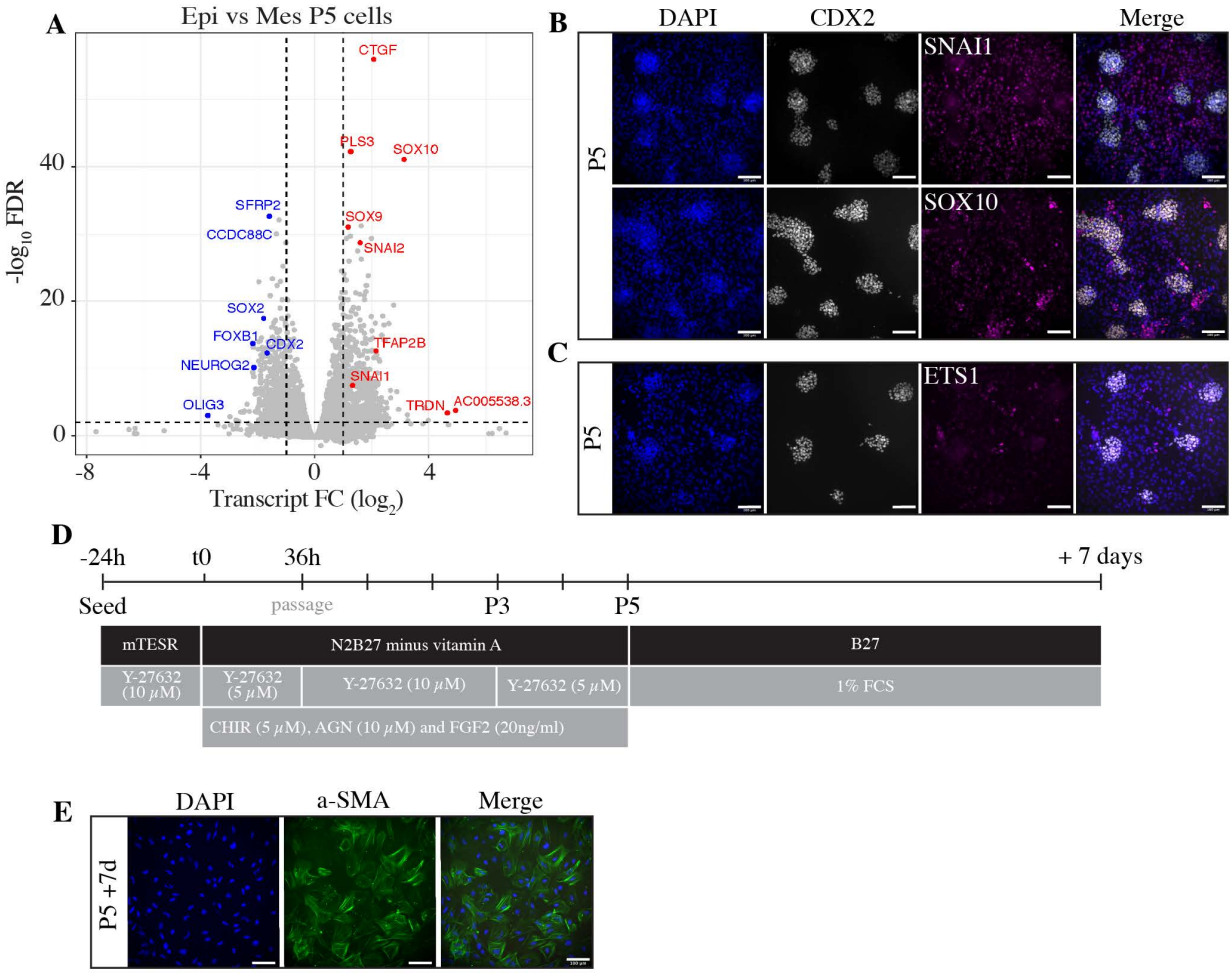

Figure 5: Mesenchymal cells have a neural crest identity.

A) Volcano plot showing differential expression between epithelial and mesenchymal cell at P5. Significant genes are highlighted in blue (epithelial) and red (mesenchymal). (B,C) Representative immunostaining of neural crest markers SNAI1, SOX10 (B) and ETS1 (C), co-stained with epithelial PNP marker CDX2 (grey) and the nuclear stain DAPI (blue). Scale bar, 100 µm. D) Scheme for generating NMP/PNP-derived neural crest derivative smooth muscle. E) Representative immunostaining of α-SMA (green) and nuclear stain DAPI (blue) in NMP/PNP-derived vasculature smooth muscle cells. Scale bar, 100 µm.

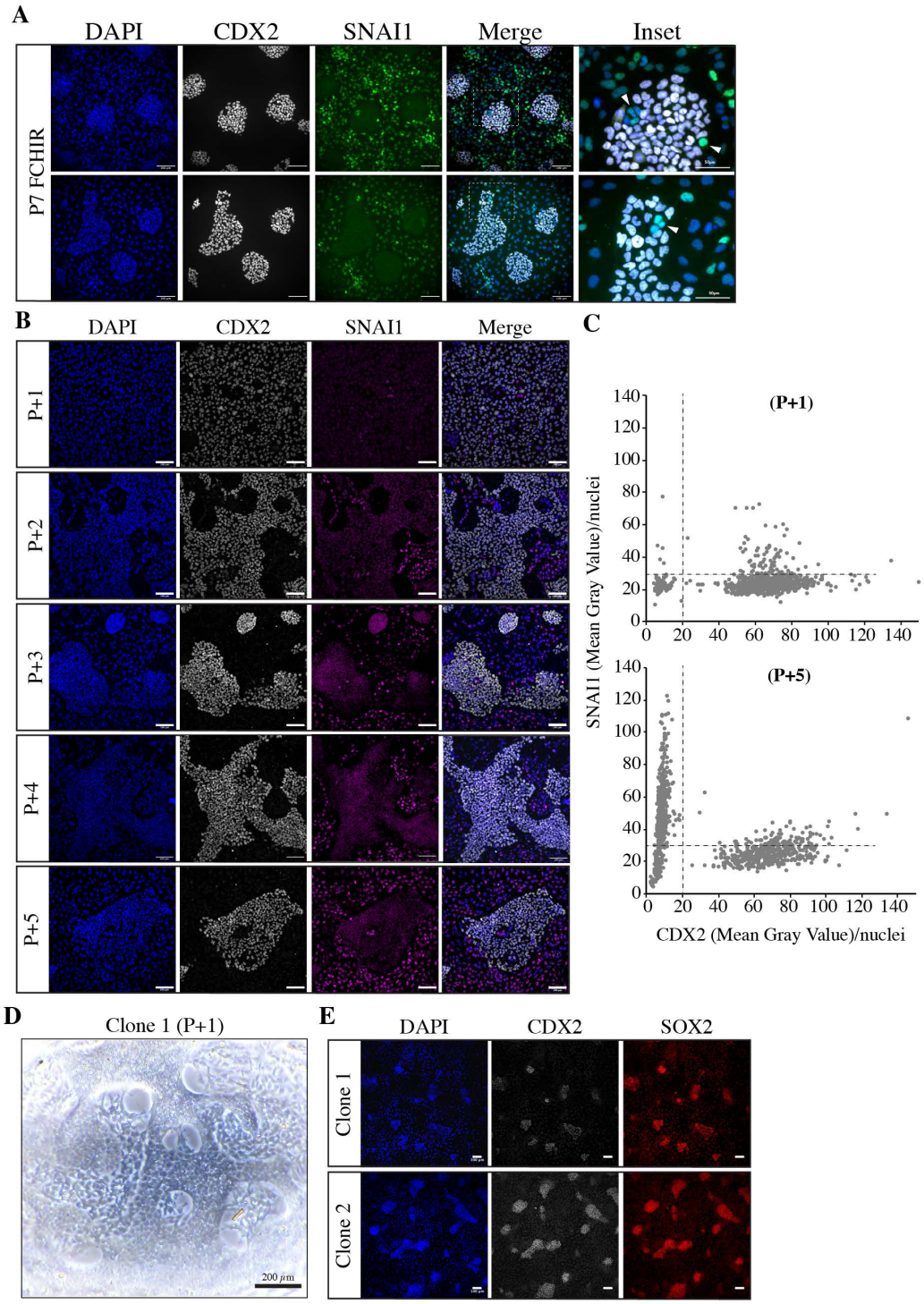

Figure 6: Epithelial PNPs give rise to migratory neural crest cells.

A) Representative immunostaining of CDX2 (grey) and SNAI1 (green) co-stained with nuclear stain DAPI (blue) in P7 PNP/NC cultures. Inset shows magnified region identified by white dashed line and arrow marks examples of CDX2$^-$/SOX2$^-$/SNAI1$^+$ nuclei within PNP clusters. Scale bars, 100µm or 50 µm (inset). B) Representative immunostaining of CDX2 (grey), SNAI1 (magenta) and nuclear stain DAPI (blue) in epithelial P5 cells which were serially passaged for four passages (P+1 to p+4) following selective detachment enrichment. (C) Dot plot showing the mean grey value/nuclei of CDX2 and SNAI1 at P+1 and P+4 panels shown in (B). Each graph shows >900 nuclei. D) Representative bright-field image of a sub-clone generated from the epithelial enriched fragment after 1 passage. Scale bar, 200 µm E) Representative immunostaining analysis of CDX2 (grey), SOX2 (red) and nuclear stain DAPI (blue) in two independent sub-clones generated from the epithelial enriched samples after serial 4 passages. Scale bar, 100 µm.

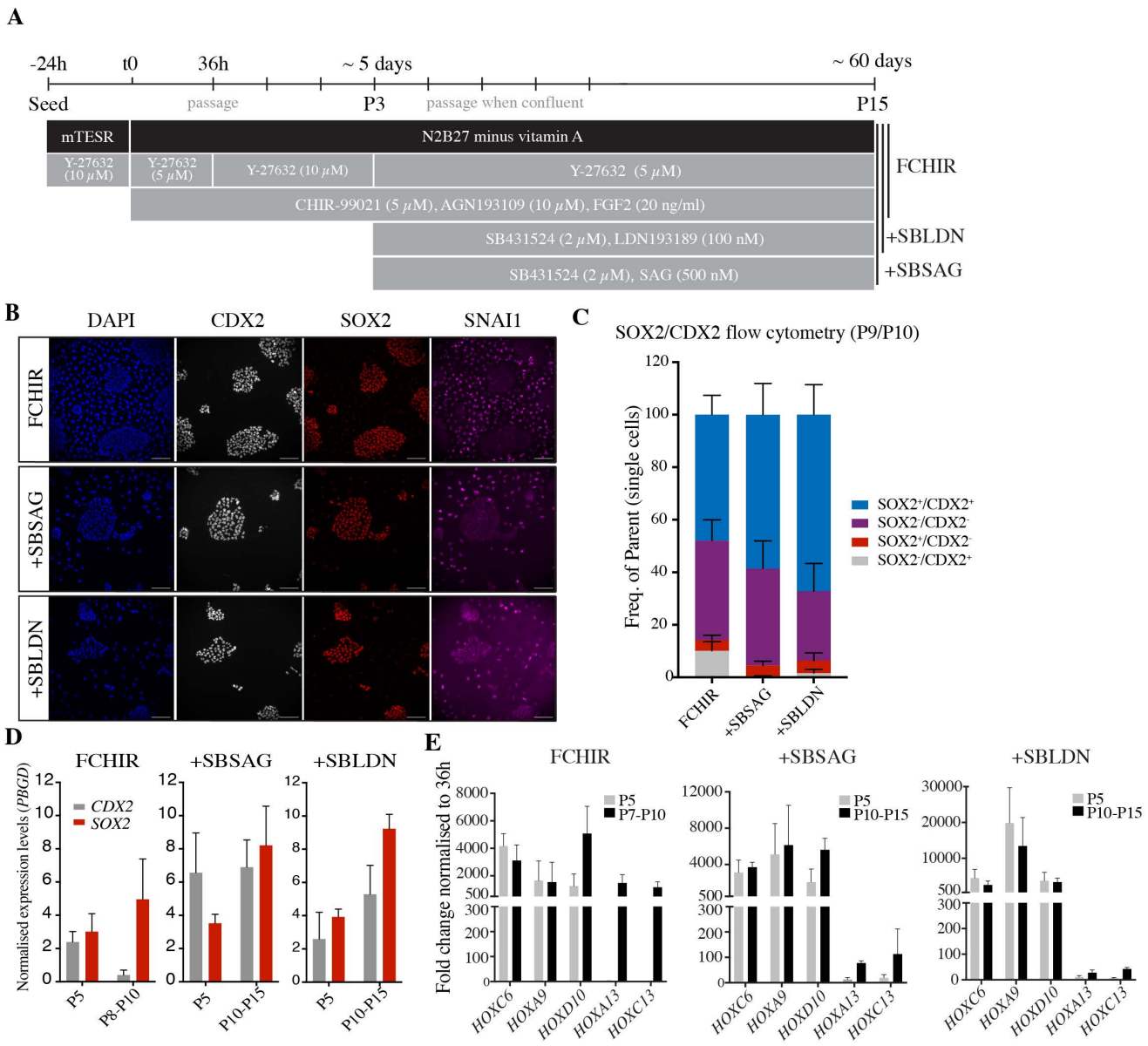

Figure 7: Modulation of TGF-β and SHH signalling locks in A/P information.

A) Scheme for generating and maintaining PNPs. At passage 3 either SB and LDN (+SB/LDN) were added, or SB and SAG (+SB/SAG) were added to the standard medium (FCHIR). B) Representative immunostaining of P5 cells for CDX2 (grey), SOX2 (red) and SNAI1 (magenta) under conditions indicated in (A). Scale bar, 100 µM. C) SOX2/CDX2 flow cytometry analysis of FCHIR (P7) and +SB/LDN and +SB/SAG (P10) samples. Cells were analysed using SOX2 and CDX2 conjugated antibodies and plotted as percentage of expression. Error bars show mean with SEM (n = 3). D) Transcriptional quantification (RT-qPCR) of CDX2 and SOX2 at early (P5) and later passages (FCHIR; P8-P10 and +SB/LDN and +SB/SAG; P10-P15). Expression levels normalised to the reference gene *PBGD.* Error bars show SEM (n = 2-5). E) Graphs showing the transcriptional quantification (RT-qPCR) of selected *HOX* genes at early (P5) and late passages (FCHIR; P8-P10 and +SB/LDN and +SB/SAG; P10-P15) in all conditions tested as indicated in (A). Expression levels are presented as fold change over the 36h time point and were normalised to the reference gene *PBGD.* Error bars show mean with SEM (n = 2/3).

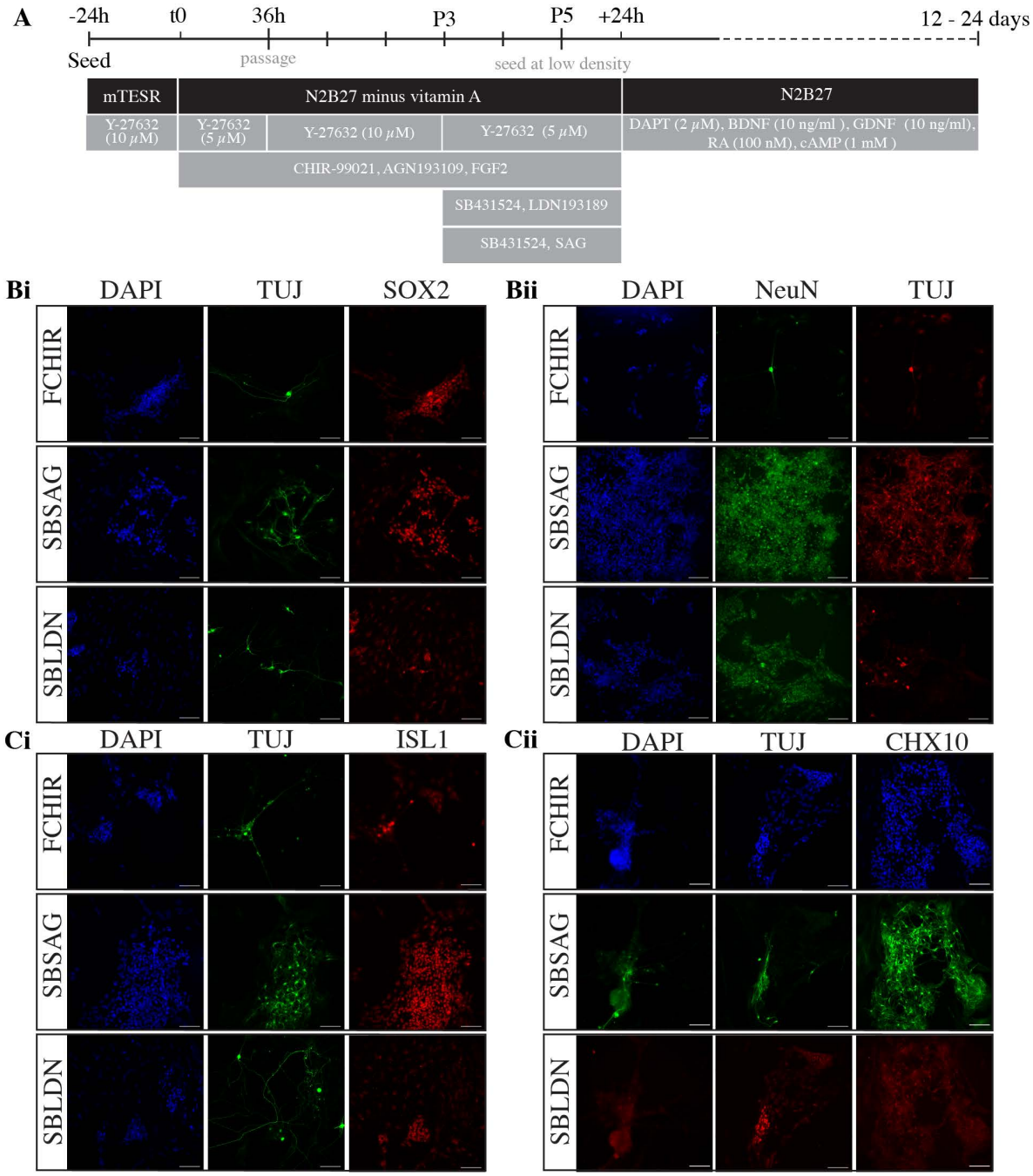

Figure 8: PNPs can be differentiated into neural derivatives and ventralised by SHH.

A) Scheme for generating differentiated neuronal cultures. Cells are grown until P5, dissociated and plated at low density and then exposed to neural inducing factors shown. B) Representative immunostaining of differentiated neuronal cultures showing (Bi) neuronal nuclei (NeuN, green) and βIII-tubulin (TUJ, red) or (Bii) SOX2 (green) and βIII-tubulin (TUJ, red). Nuclei were stained with DAPI (blue). Scale bars, 100µm. C) Representative immunostaining of ventral neurons stained with ISL1 (red, Ci) and CHX10 (red, Cii) paired with βIII-tubulin (TUJ, green) and nuclear stain DAPI (blue). Scale bars, 100µm.

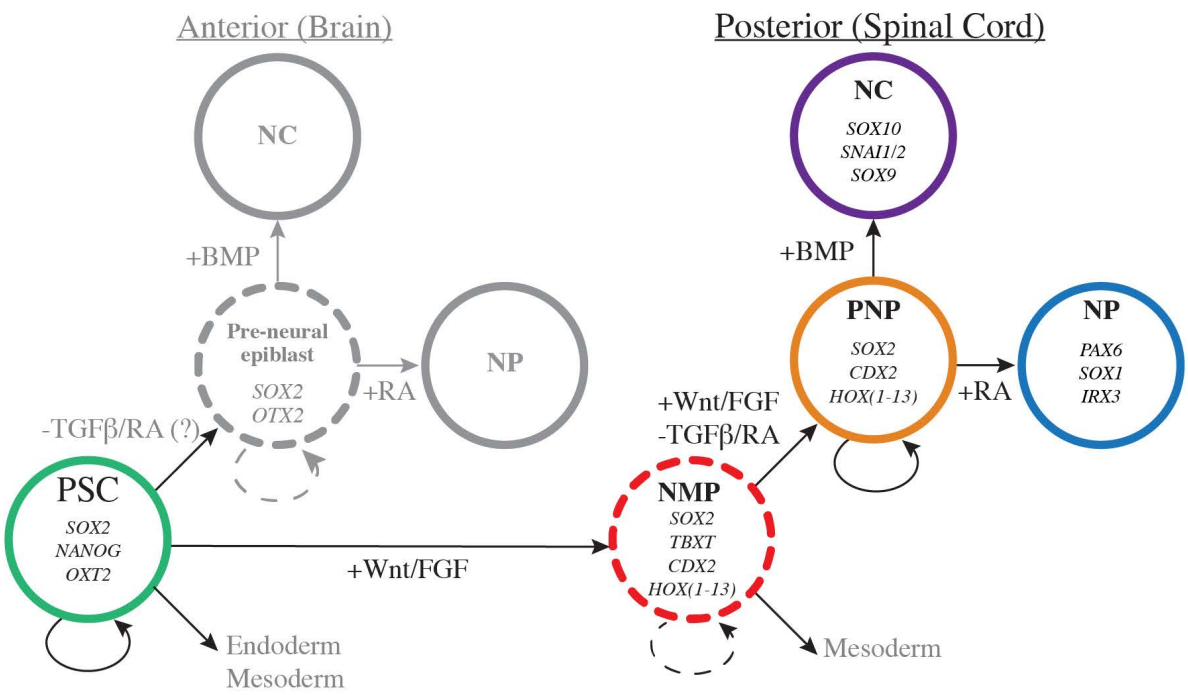

Figure 9: NMP-derived PNPs self-renew, give rise to trunk NC or can be differentiated to neurons. Diagrammatic model summarising the generation of anterior (brain) and posterior (spinal cord) neural progenitors *in vitro*. When treated with inhibitors of TGFβ signalling pluripotent stem cells (PSC) in the give rise to a transient pre-neural epiblast state, which in turn give rise to anterior neural crest (NC) and neural progenitors (NP) of the brain. Neuromesodermal progenitors (NMP), which give rise to posterior neural tissue, are generated from PSC in response to Wnt/FGF signalling. In the absence of RA and TGFβ signalling, NMPs differentiate to a stable pre-neural progenitor (PNP) intermediate which are able to self-renew and give rise to neural progenitors when subjected to RA or neural crest in the presence of BMP. Transient cell states are shown using dotted lines and cells with self-renewal capacity are shown with curved arrows.

1056 **SUPPLEMENTARY FIGURES**

A

Paper:	CHIR-99021:	FGF:	Treatment time:	Plating density:	Recovery time after plating:	Additional molecules:
Frith et al., (2018)	3-4 μM	FGF2 (20 ng/ml)	72h	55,000 cells/cm^2	0h	
Gouti et al., (2014)	3 μM	FGF2 (20 ng/ml)	72h	80,000 cells/cm^2	0h	
Verrier et al., (2018)	3 μM	FGF2 (20 ng/ml)	72h	40,000 cells/cm^2	24h	
Lippman et al., (2016)	2-3 μM	FGF8b (200 ng/ml)	72h (FGF 24h, FGF + CHIR 48h)	100,000 cells/cm^2	24h	
Denham et al., (2015)	3 μM	None	96h	Aggregates	0h	SB-431542 (10 μM)
Wang et al., (2019)	10 μM	FGF2 (20 ng/ml)	48h	20,000 cells/cm^2	0h	TGFβ1 (2-5 ng/ml)
Kumamaru et al., (2018)	4 μM	FGF2 (100 ng/ml) FGF8b (100 ng/ml)	72h	70% confluence	N/A	LDN-193189 (100 nM) SB-431542 (10 μM) DAPT (10 μM)
Gomez et al., (2019)	10 μM	None	24h-48h	200,000 cells/cm^2	0h	

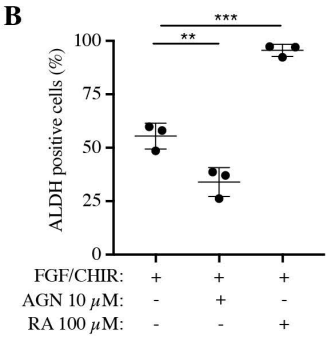

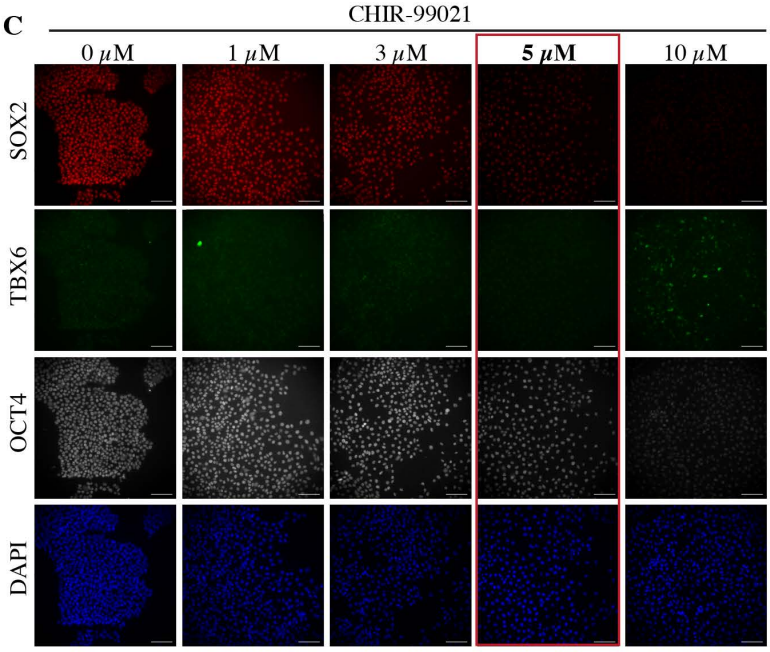

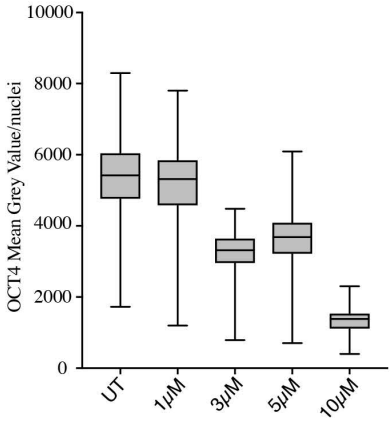

1057 **Figure 1 – figure supplement 1: NMP-like cells are induced by combined Wnt/FGF and inhibited RA**
1058 **signalling.**
1059 A) Summary of protocols used in recent studies to generate NMP-like cells from hPSCs. Table includes
1060 plating density and recovery time after plating, as well as the exogenous molecules and treatment
1061 time used. B) ALDEFLUOR assay was used to measure the expression of aldehyde dehydrogenases
1062 (ALDH) in 36h samples generated in three conditions: 1) FGF2 and CHIR only, 2) FGF, CHIR and AGN or
1063 3) FGF, CHIR and RA. Samples were analysed using flow cytometry and results were presented as the
1064 percentage of cells expressing ALDH. Error bars show SD (n = 3 experiments). **P <0.01, ***P <0.001
1065 (ANOVA). C) Representative immunostaining SOX2 (red), TBX6 (green) OCT4 (grey) and the nuclear
1066 stain DAPI (blue) after 36h treatment following scheme as shown in Figure 1A with 0 µM, 1 µM, 3 µM,
1067 5 µM and 10 µM CHIR-99021. Scale bars, 100 µm. D) Box-plot showing mean grey value/nuclei
1068 quantified from repeat experiments as shown in (C). Plot show data points collected from 2
1069 experiments (>450 nuclei/experiment).

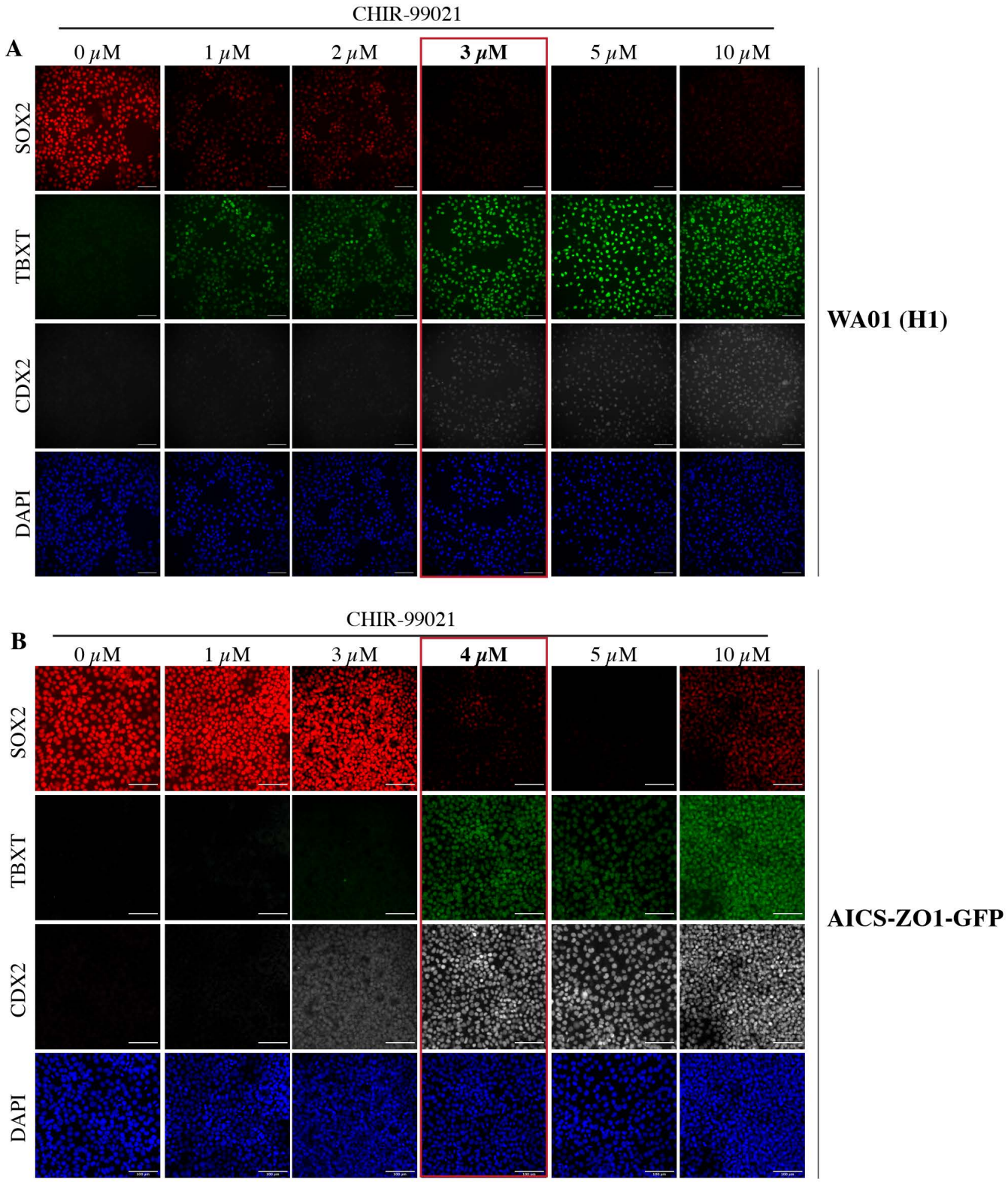

Figure 1 – figure supplement 2: Generation of NMP-like cells in multiple hPSC lines requires modulation of the Wnt pathway.

A, B) Optimal CHIR concentration was optimised for WA01 (H1) hESCs (A) and AICS ZO1-mEGFP (AICS-0024) iPSCs (B). Representative immunostaining of NMP markers SOX2 (red) and CDX2 (grey) and TBXT (green) at 36h after following treatment scheme shown in Figure 1A, with a range of CHIR concentrations between 1-10 μM. Scale bars, 100μm.

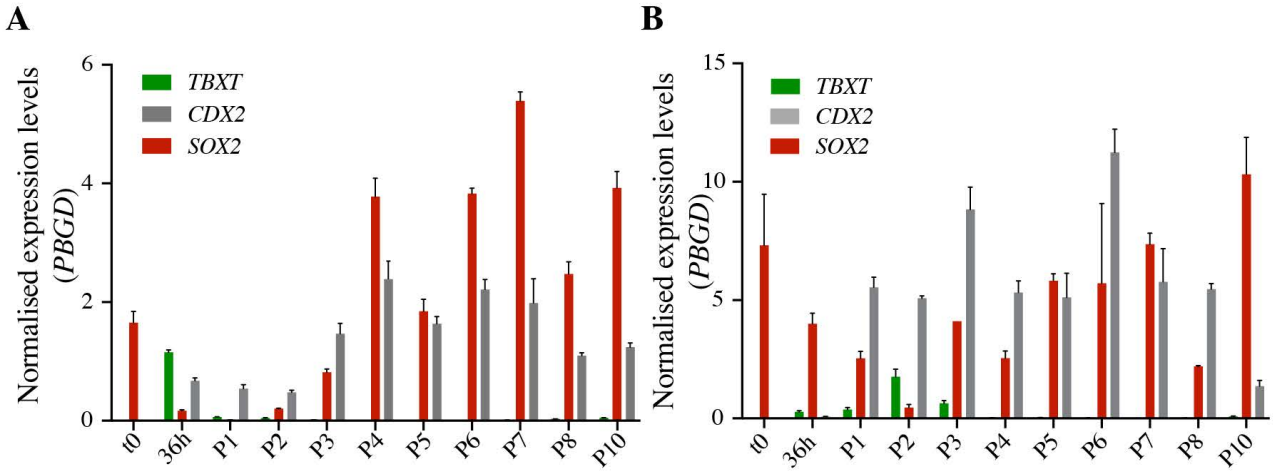

1076 **Figure 2 – figure supplement 1: CDX2 and SOX2 expression can be maintained for 10 passages.**

1077 A,B) Transcriptional analysis (RT-qPCR) of two independent experiments showing NMP markers *TBXT,*
1078 *SOX2* and *CDX2* at each passage, up to passage 10. Expression levels are normalised to the reference
1079 gene *PBDG*. Error bars show SD, (n=3 technical replicates).

1080

1081

1082

1083

1084

1085

1086

1087

1088

1089

1090

1091

1092

1093

1094

1095

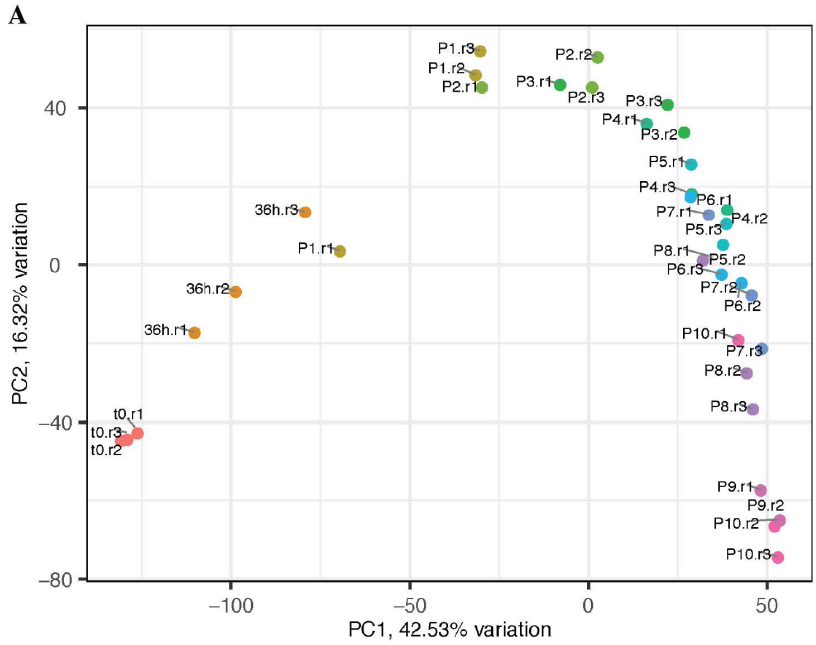

Figure 3 – figure supplement 1: Principle component analysis of RNA-Seq samples collected over passaging.

A) PCA analysis show biological replicates for each passage cluster together and show small biological variation between experiments

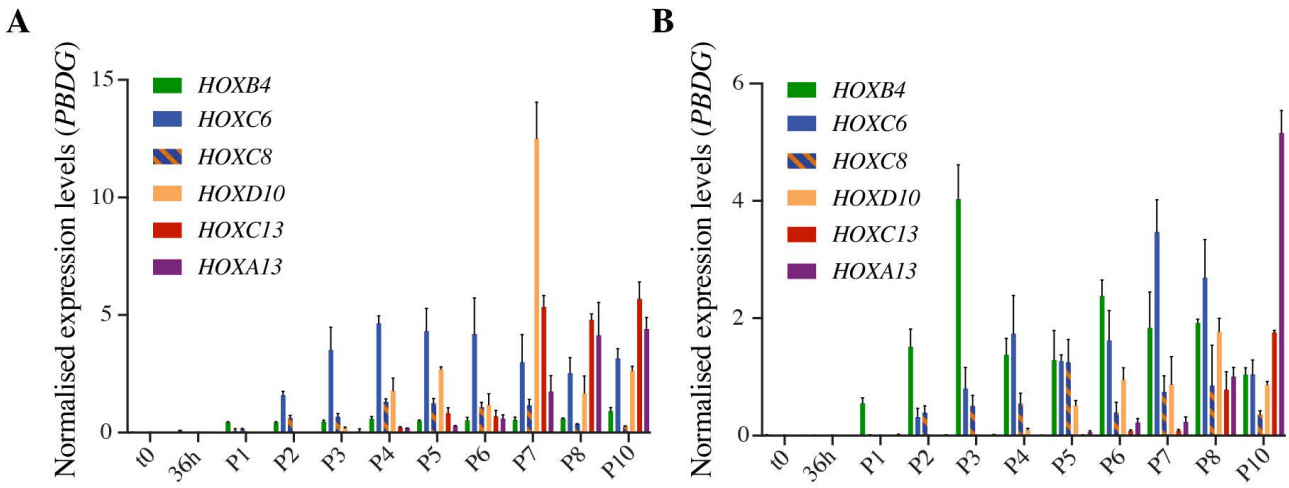

Figure 3 – figure supplement 2: Full collinear expression of the HOX gene cluster occurs over 10 passages.

A,B) Transcriptional analysis (RT-qPCR) of two independent experiments showing selected HOX genes at each passage up to passage 10. Expression levels are normalised to the reference gene *PBDG*. Error bars show SD, (n=3 technical replicates).

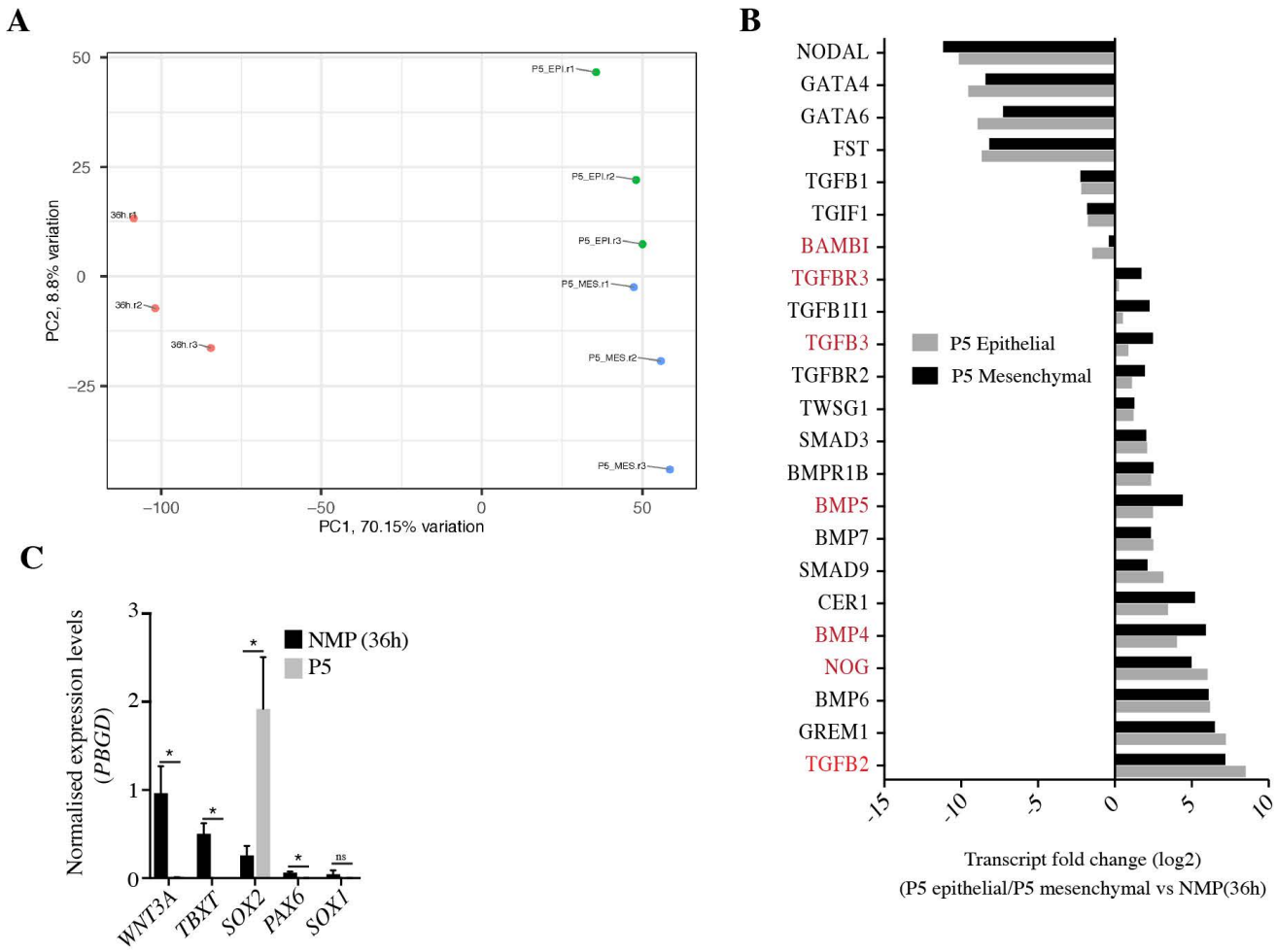

Figure 4 – figure supplement 1: Principle component analysis of mesenchymal and epithelial samples analysed by bulk RNA-sequencing.

A) PCA analysis showing biological replicates for the mesenchymal (MES) and epithelial (EPI) enriched samples and NMP samples (36h). B) Graph showing transcriptional fold change (FC) of selected TGF superfamily genes in P5 epithelial and P5 mesenchymal samples over 36h samples. Genes which are statistically differentially expressed between epithelial and mesenchymal samples are highlighted in red. C) Transcript levels of *WNT3A, TBXT, SOX2 PAX6* and *SOX1* in NMP (36h) and P5 samples as measured by RT-qPCR. Expression levels were normalised to the reference gene *PBGD*. Error bars show SEM (n=2/3 experiments), *P <0.05 (unpaired t-test).

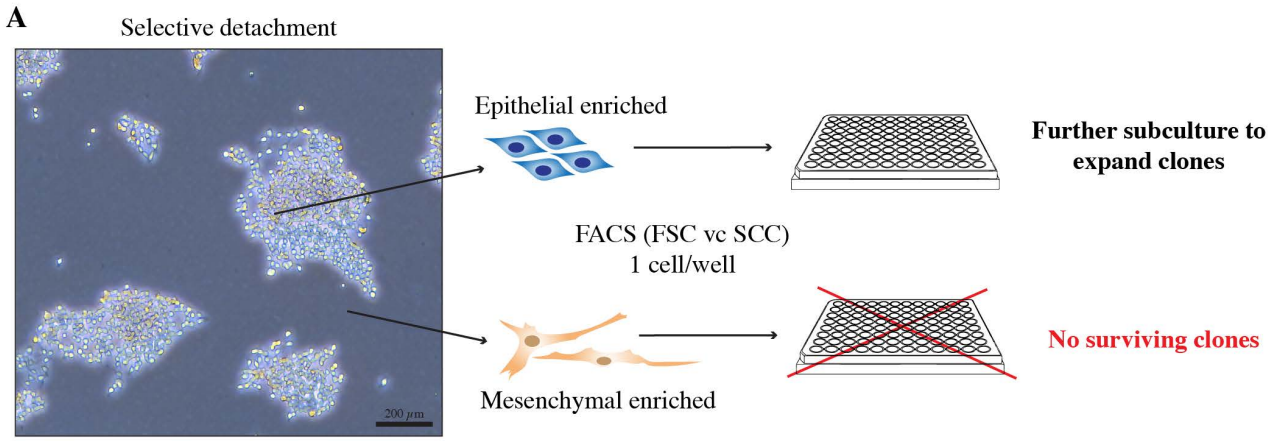

Figure 6 – figure supplement 1: Generating sub-clonal populations from PNP/NC cell enriched samples

A) Scheme to generate sub-clonal populations from mesenchymal- or epithelial- enriched samples. Cells were selectively detached to separate epithelial from mesenchymal cell populations and single cells from each enriched cell sample were sorted (FACS) into wells of a 96 well plate. Surviving sub-clones were expanded for analysis.

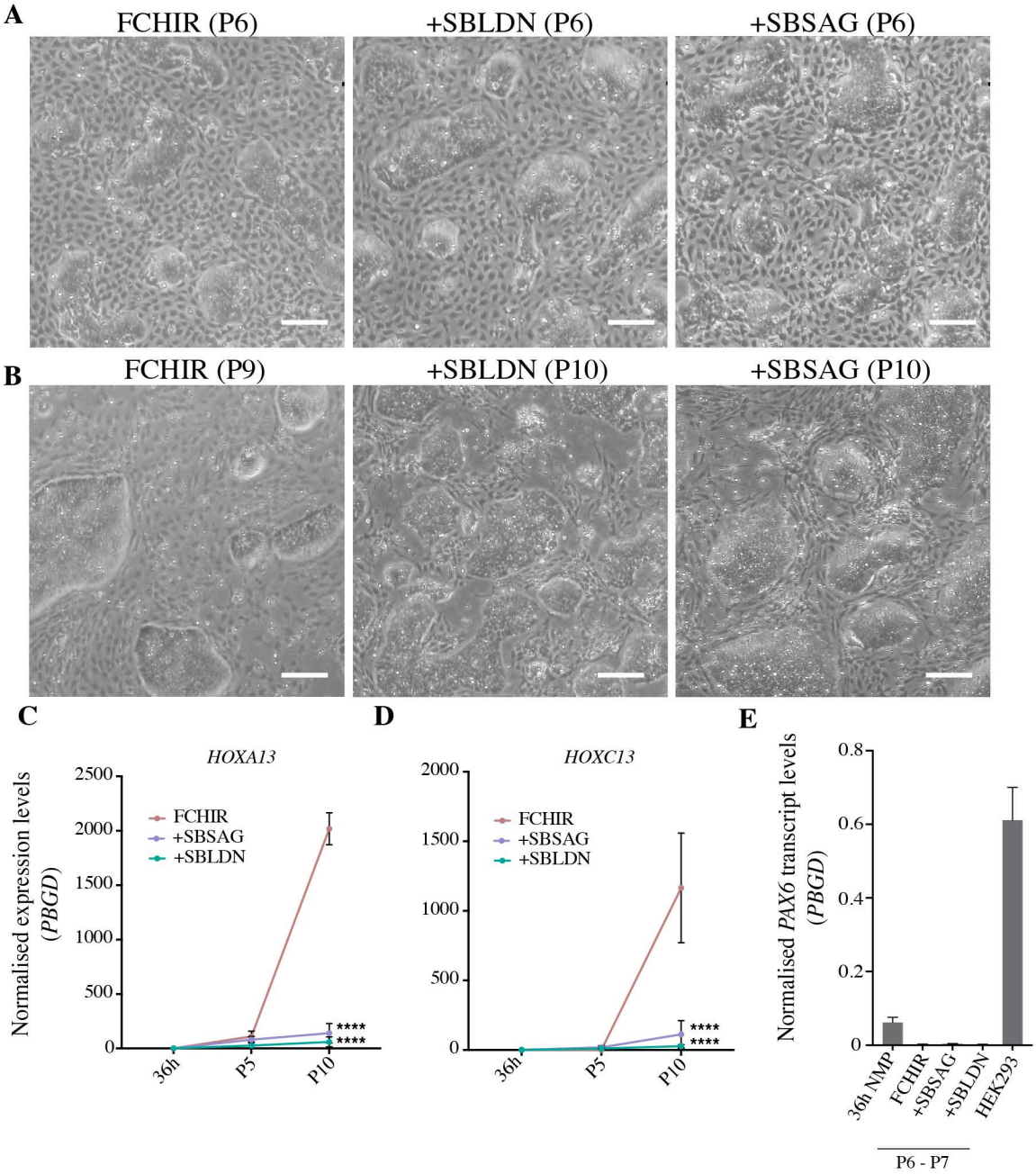

Figure 7 – figure supplement 1: Upregulation of terminal *HOX* genes is significantly delayed, and neural marker gene *PAX6* remains silent, in +SBSAG and +SBLDN conditions

A, B) Graphs showing the transcriptional quantification (RT-qPCR) of *HOXA13* (A) and *HOXC13* (B) at early and late passages in all conditions tested as indicated in Figure 7A. Expression levels are presented as fold change over the 36h time point and were normalised to the reference gene *PBGD.* Error bars show mean with SEM (n = 3). ****P<0.0001, ***<0.0002 (two-way ANOVA). C) Quantification of *PAX6* transcript levels under various conditions as indicated in Figure 7A, and in comparison to HEK293 (positive control) cells. Expression levels were normalised to reference gene *PBGD.* Error bars show mean with SEM (n = 2-3).